THESIS

CHARACTERIZATION OF CHROMATIN REMODELING IN MESENCHYMAL STEM CELLS ON THE APPLICATION OF OXIDATIVE STRESS

Submitted by

Neda Kabi

School of Biomedical Engineering

In partial fulfillment of the requirements

For the Degree of Master of Science

Colorado State University

Fort Collins, Colorado

Fall 2022

Master's Committee:

Advisor: Soham Ghosh

Ketul Popat
Laurie Goodrich
Brian Johnstone

ABSTRACT

CHARACTERIZATION OF CHROMATIN REMODELING IN MESENCHYMAL STEM CELLS ON THE APLLICATION OF OXIDATIVE STRESS

Chromatin is a highly dynamic entity of the eukaryotic cell nucleus. Contrary to previous belief that chromatin maintains a well-defined permanent architecture in the interphase nucleus, new evidences are emerging with a support of the notion that chromatin can locally and globally rearrange itself to adapt with the cellular microenvironmental changes. Such microenvironmental changes can be related to biophysical such as change in the stiffness of extracellular matrix or the force applied on the cell as well as biochemical such as change in the oxidative stress, osmolarity or the pH. It is not well understood how the chromatin architecture changes under such environmental changes and what is the functional significance of such change. Characterization and quantification of chromatin remodeling is therefore a first step to understand the chromatin dynamics for elucidating complex subnuclear behavior under the influence of single or multiple environmental changes. Towards that end, in this work, human bone marrow derived mesenchymal stem cells were used to characterize such chromatin level changes under the changing oxidative stress on the cells. Oxidative stress was applied using hydrogen peroxide treatment. After validation of the application of oxidative stress, a series of experiments and subsequent analysis was performed to understand the hallmarks of chromatin remodeling at high spatiotemporal resolution. Specific chromatin remodeling pattern was observed in the heterochromatin,

euchromatin and the interchromatin regions. Finally, a key component of chromatin remodeling complex called ARID1A was identified which is critical for the chromatin remodeling process.

ACKNOWLEDGEMENTS

I would first like to thank my advisor, Dr. Soham Ghosh, for his exceptional guidance and persistent support throughout my time in graduate school. His unmatched wisdom and dedication to research serves as personal inspiration for all his students and mentees. My gratitude also extends to my laboratory colleague, Samantha Kaonis. She and I shared many of the same experiences and the journey would not have been the same without her. I also thank several Ghosh Lab members: Abigail Fennell, Lauren Monroe and Jack Forman for their technical contribution in multiple aspects during the execution of this project. Lastly, I would like to acknowledge my parents and my partner, for their continued encouragement and unconditional love in every chapter of my life.

DEDICATION

I dedicate this to my advisor, Dr. Soham Ghosh, who took a chance on me, inspired me, and never gave up on me.

TABLE OF CONTENTS

LIST OF TABLES

LIST OF FIGURES

CHAPTER 1

LITERATURE REVIEW

1.1 Cell nucleus and chromatin architecture

The eukaryotic cell nucleus (Figure 1.1) is a lipid bilayer membrane bound organelle (1–3) that contains, maintains and interprets genetic information in the chromatin architecture. It also separates the intranuclear space from the cytoplasm.

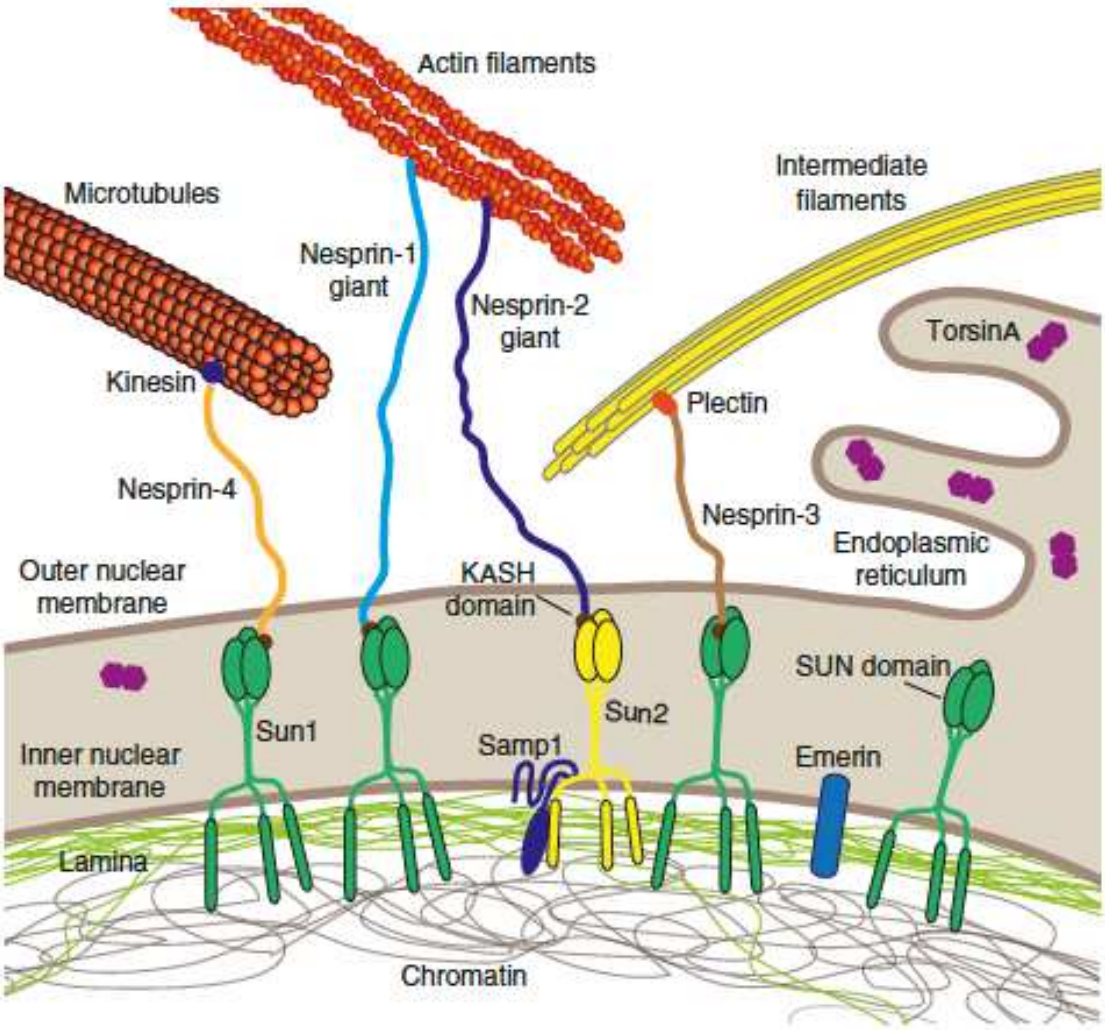

Figure 1.1 Essential components of an eukaryotic cell nucleus (1) at the nucleus-cytoplasm interface. The key structural components are only shown in the figure [from Isermann et al., 2013, Current Biology(1)].

The two layers of the nuclear membrane are the Inner Nuclear Membrane (INM) and the Outer Nuclear Membrane (ONM). The intranuclear space consists of the chromatin architecture, the nucleoplasm - made of a nucleoskeleton structure and liquid nuceosol, and several other specialized organelles such as nucleolus. The protein coding and non-coding regions of DNA are the fundamental units of the chromatin architecture. In interphase (non-dividing) cell nucleus plenty of proteins are localized above, inside and under the nuclear membranes to build the Nuclear Envelope (NE). The chromatin architecture does not just float in the nucleoplasm, rather it is connected to the NE through several structures. One such important structure is the mesh-like nuclear lamina which resides under the INM. Nuclear lamina consists of the intertwining network of Lamin A/C, Lamin B1 and Lamin B2. Another important structure is the LINC complex (LInker of Nucleoskeleton and Cytoskeleton) consisting the SUN (Sad1p, UNC-84) and KASH (Klarsicht, ANC-1, Syne Homology) domains. LINC complex is connected to the cytoskeleton (actin, intermediate filament, microtubule) via different types of nesprin. Inside the nucleus, the LINC complex and the nuclear lamina are physically connected to the chromatin through many proteins such as the LAD (Lamina Associated Domain) LEM (LAP2-Emerin-Man1) domains, LEM like domains and LBR (Lamin B Receptor).

The chromatin architecture is intricately packed to fit a two-meter-long DNA strand into approximately three hundred cubic micrometers of nuclear volume (4–7). Of course, the packing is extremely dense, but it is not random. It is ensured that despite such intricate and dense packing, a gene is efficiently transcribed in this crowded environment if a biological function demands so. The intricate packing is facilitated by spatially hierarchical mechanisms involving DNA methylation, histone modifications, chromatin remodeling complex mediated chromatin remodeling and long-range chromatin modifiers (4, 8). Some of these mechanisms are termed as

epigenetic regulators because those mechanisms do not directly change the genetic code and they might be heritable after the cell goes through cell division (8, 9). The result of the complex packing by diverse mechanisms lead to a heterogeneous chromatin architecture with spatially heterogeneous mechanical properties (10). It is densely packed ('close' conformation) in some regions of the nucleus, termed heterochromatin (HC) which contains repressed genes (11, 12). On the contrary, it is loosely packed ('open' conformation) in some regions, called euchromatin (EC) containing the transcriptionally active genes. However, EC and HC regions are not clearly demarcated resembling perennial 'ON' or 'OFF' states. EC can be **remodeled** into HC and *vice versa*. Another zone called 'interchromatin' (IC) is being recognized more recently which is the region between the HC and IC. Current understanding and state of the art suggests that IC region is critical in the regulation of HC to IC conversion and *vice versa* and might have elaborate biological role to determine the chromatin function(13).

1.2 Chromatin remodeling

Chromatin remodelers are thought to control the opening and closing of the chromatin architecture and therefore, the transition from euchromatin to heterochromatin and vice versa. The chromatin architecture at any given region in the nucleus can be dynamically opened or closed by the 'Chromatin Remodeling Complex' or CRC. CRC is a highly conserved mechanism in the eukaryotic cells. Figure 1.2 explains the process for chromatin opening by CRC. The understanding of the molecular biology of CRC grew rapidly in the last 20 years (14–17). The core component of this complex is a core protein (e.g. BAF250A/B or ARID1A/B) with an ATPase domain which is responsible for the chromatin remodeling by directly interacting with the nucleosomes (the core unit on which DNA strand is wrapped around) in the chromatin. The core protein is flanked by several component accessory proteins (e.g. BRG1/BRM and others) which

are required for the CRC to be assembled and functional. Detailed characterization of the components has been done by structural biologists and the function of each component is now being elucidated by loss of function studies. In mammals there are four families of CRC classified based on the nature of the core component protein (14). They are called as SWI/SNF, ISWI, CHD and INO80 families. Each family has some common structural features with the other families, just like Lamins A, C, B1 and B2 have common features. (SWItch/ Sucrose Non-Fermentable) SWI/SNF is the most investigated among all the types and it is specifically known to unwrap chromatin and make genes accessible to the transcriptional factors, by nucleosome sliding and ejection (18–22). Recent discoveries indicated that in cancer and degenerative diseases, SWI/ SNF is inactivated or mutated (23–32). The current state of the knowledge suggests that CRC members can be critical in rapid or slow chromatin remodeling.

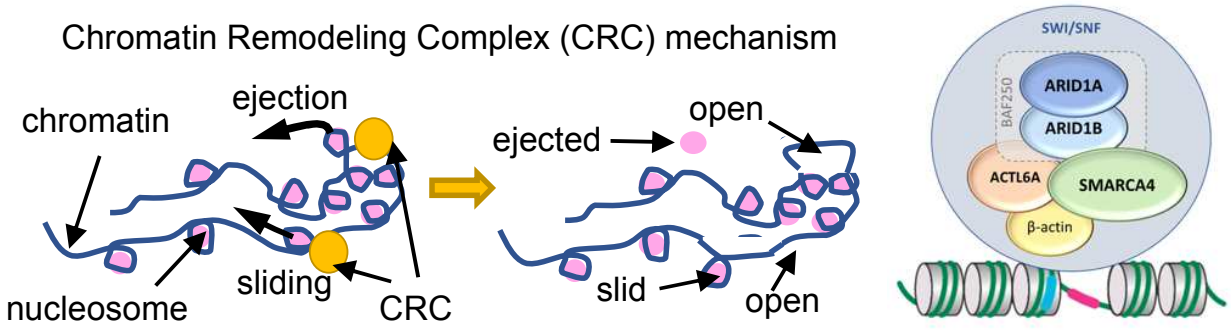

Figure 1.2 (a) SWI/SNF Chromatin Remodeling Complex (CRC) is a thoroughly investigated chromatin remodeler. The current understanding states that its activation and engagement open the chromatin to facilitate the chromatin remodeling. (b) It has many subunits including ARID1A which is the focus of the present study. Other subunits are also critical for the function of the CRC.

1.3 Oxidative stress in cells and mesenchymal stromal/ stem cells

Mesenchymal Stromal/ Stem Cells (MSC) are activated *in vivo* and *in vitro* under physiological stress. From multiple lines of evidence, it was suggested that the MSC are deployed for regeneration(33, 34) when the tissue they are residing in is physiologically stressed, as seen in

degenerative conditions associated with aging and diseases such as osteoarthritis and bone injury. In fact, stress inducing hypoxic condition has been exploited to mobilize and activate MSC for enhanced regeneration *in vivo*(35–37). Since no technology currently exists to directly investigate the stress response or to even visualize individual MSC *in vivo*(38, 39), the stress response has been investigated using a reductionist *in vitro*(33) approach. Stress inducing physiological conditions include oxidative condition, mechanical stretch and metabolic stress. Under these conditions, MSC show higher activation, differentiation and proliferation(40–48). However, at higher passages and by prolonged stress events, the MSC become 'aged' or senescent. Maintenance of optimal oxidative status is critical for tissues to survive and regenerate during its lifetime(49–52). Oxidative stress in the form of Reactive Oxygen Species (ROS) is produced as a product of normal metabolism and other mechanisms. Oxidative stress is particularly relevant to stem cells and specifically MSC because it damages cellular macromolecules, including DNA, resulting in both apoptosis and cellular senescence(51). With aging and tissue degeneration, the oxidative stress increases. Concomitantly, antioxidants stimulate MSC survival and proliferation(53).

1.4 Chromatin architecture and oxidative stress

Cells possess several protective mechanisms to combat environmental stress. Such environmental stress is common in culture conditions *in vitro* and also *in vivo*(54). A common downstream effect of such environmental stress is DNA damage(33, 55, 56). In epithelial and other cells, the chromatin is shown to remodel for protecting the nucleus from the adverse effects of the DNA damage lesion(57–60). DNA damage is known to soften the chromatin architecture to either create a protective dense heterochromatin barrier to stop the damage response spreading into the nucleus, or the damaged DNA lesion may be carried to an open euchromatin region for efficient damage

correction(60, 61). However, it is not understood what are the steps post DNA damage which facilitate such chromatin remodeling. Investigation of those mechanism and exploitation of those mechanism is the long-term goal in my advisor Dr. Ghosh's lab at Colorado State University. This thesis attempts to create the technical and conceptual framework of that long term plan.

1.5 Outstanding knowledge gap

Although it is clear that MSC undergo senescence in vitro and in vivo under physiological stresses including oxidative stress, it is not clear what protective mechanisms the MSC or any other cells display at the chromatin level to slow down or repair the DNA damage lesions. Particularly it is unknown whether chromatin remodeling happens at all, what is its dynamics and what are the key mediators of this process. This thesis will address the development of techniques to visualize post-stress chromatin response in MSC and find the potential mediators of such chromatin remodeling which involve the chromatin remodeling complex proteins.

CHAPTER 2

CHARACTERIZATION OF CHROMATIN REMODELING IN MSC ON THE APPLICATION OF OXIDATIVE STRESS

2.1 INTRODUCTION

Mesenchymal Stromal/ Stem Cells (MSC) exist in the bone marrow and many other tissues. The current understanding is that MSC are a part of the 'stroma' and they are an integral part of any vascularized tissue and they originate from the pericyte in the blood vessel(62). Traditionally, MSC have been cultured and engineered after extraction from bone marrow and adipose tissue for intended therapeutic purpose. MSC can be differentiated into many cell and tissue types *in vitro*, which are further used for tissue engineering purpose. Although *in vivo* natural differentiation of MSC have never been confirmed, MSC are thought to have regenerative benefits naturally *in vivo* and upon injection inside the tissue after *ex vivo* expansion. MSC are often exposed to oxidative conditions *in vitro* and *in vivo* during the culture, upon transplantation and during their *in vivo* natural regeneration(63). Oxidative stress is known to cause DNA damage and genomic instability(64, 65). However, it is not clear for any cell what are the key physical and biological events at the chromatin level that follow the oxidative stress and/ or the DNA damage and what molecules are potential mediator of the DNA damage correction through chromatin remodeling. Understanding such mechanism might provide us with new mechanism and intervention strategies to target genotoxic stress which is common in degenerative diseases and aging. Subsequently, the following two hypotheses were proposed in this study using the model cell of MSC for their natural niche of oxidative stress rich environment(63).

Hypothesis 1: Different chromatin regions such as heterochromatin, euchromatin and interchromatin show differential response to the DNA damage during the chromatin remodeling (heterochromatin, euchromatin and interchromatin are explained in detail in chapter 2)

Hypothesis 2: ARID1A (a subunit of SWI/SNF chromatin remodeling complex) is a potential mediator of the chromatin remodeling (SWI/ SNF complex is explained in detail in chapter 1)

Subsequently, to test the above hypotheses, our **objectives** were –

(1) To characterize and quantify the chromatin remodeling in high spatiotemporal resolution post DNA damage using hydrogen peroxide induced oxidative stress

(2) To identify the role of ARID1A in chromatin remodeling using ARID1A inhibitor GSK126

To execute the above objectives, we used passage 5 bone marrow derived MSC (Lonza) for all the studies. Cells were either treated with ARID1A inhibitor GSK126 or non-treated (control). First, cell proliferation and viability were investigated to understand the effect of GSK126 on MSC. Subsequently, cells were exposed to hydrogen peroxide treatment. Live imaging and image analysis were performed to understand the effect of hydrogen peroxide and the ARID1A in the spatiotemporal chromatin remodeling. The viability of MSC upon oxidative stress and upon ARID1A inhibition further elucidates a functional role of ARID1A upon MSC exposure to oxidative stress.

2.2 MATERIALS AND METHODS

Cell culture

Human bone marrow derived MSC (BM-MSC) were used for this study. Cells were obtained from Lonza at passage 2 (PT-2501), which are BM-MSC from healthy adults. Cells were subcultured using Lonza MSC general medium (MSCGM) consisting MSC basal medium and growth supplements (MCGS) at 37°C, 90% humidity and 5% CO_2. DPBS and 0.025% Trypsin

EDTA (Thermo Fisher) were used for the washing and passaging purpose. For all live experiments, cells were maintained at the MSCGM. For all imaging experiments we used ibidi 8 well μ-slides (ibidi 80826) which are tissue cultured treated and consists of a #1.5 polymer coverslip at the bottom. 300 μL of MSCGM was used for each well. Cells were seeded at 8500/ cm^2.

Drug treatment

Cells were exposed to drug after 1 day when cells were well attached. ARID1A inhibitor GSK126 (Sigma Aldrich) was mixed with the complete culture medium at 20 μM concentration. The control groups contained DMSO (2 μl/ ml) to match the concentration of the drug's dilutant which is also DMSO (VWR). After 4 days of drug treatment all the subsequent experiments were performed. At the day 2 of drug treatment (or control), medium was changed so that cells remain healthy and viable.

Quantification of cell proliferation

After 5 days of complete cell proliferation (1 day pre drug treatment for attachment, 4 days post drug treatment) cells were imaged under a confocal microscope. Bright field images (2.5X) were obtained using the transmitted light and camera of the confocal microscope. For counting cells, the cells were exposed to Nucblue (1 drop per ml of complete culture medium: control or with drug). After incubation of 20 minutes at 37°C, 90% humidity and 5% CO_2 the live cells were imaged (2.5X) to visualize the cell nucleus. Subsequently, the images were threholded in ImageJ and particle analyzer was used to count the number of cells in each field of view which is at the middle of the 8 well slide – the position is automatically calculated using the microscope's calibration menu. That number was used to extrapolate the cell number per unit area of the well (1 cm^2). Then the initial cell seeding number (8500/ cm^2) was used to calculate the fold change of cell number at day 5 compared to the day 1 of cell seeding.

Quantification of cell viability

Cell viability after the drug treatment was performed using a commercial live/dead assay kit consisting calcein AM and ethidium homodimer. Live cells were exposed to the content of the kit (calcein AM: 1 μM and ethidium homodimer: 4 μM) at 37°C, 90% humidity and 5% CO_2 for 40 minutes before the cell imaging. Cells were imaged using confocal microscope in the 488 nm (green) and 561 nm (red). The concentration of the content of the kit was previously optimized using a standardized technique for BM-MSC. The viability assay was validated by killing all the MSC using 70% methanol with 30 minutes of exposure inside the cell culture incubator.

Hydrogen peroxide treatment and its validation

To understand the live response of MSC nucleus to Hydrogen peroxide the H_2O_2 (Sigma) was diluted in the DPBS (10 mM) and further diluted at 500 μM concentration in the MSCGM (with or without drug GSK126).

To validate the oxidative stress of the hydrogen peroxide treatment the cells were exposed to H_2O_2 at different concentrations (0 μM, 100 μM, 200 μM) for 24 hours. Cells were then stained with CellROX Green for 30 minutes, fix cells with 4% paraformaldehyde and counterstained with DAPI (DNA stain). The cells were then imaged using the confocal microscope (20X). This step was used only to validate the response of cells to H_2O_2, and therefore the experiment was never performed at a higher concentration of 500 μM. Independently, my colleague Samantha Kaonis used RT-qPCR and found that on H_2O_2 application, expression of signatures genes increases. Average intensity of the green channel was calculated after separating the blue and green channels as the green channel shows the CELLROX stain.

Live imaging of chromatin remodeling and nuclear area change

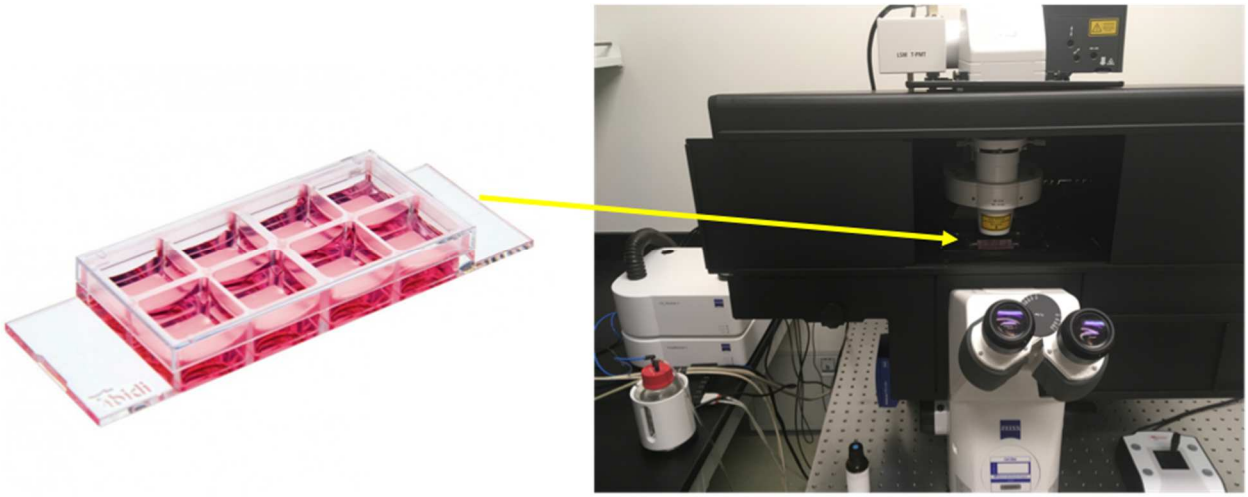

Figure 2.1 Ibidi 8 well plate was used for all imaging work of this study. The plate was placed inside the confocal microscope for all imaging purpose.

The cells were ready for imaging after 5 days in culture and at that timepoint, NucBlue was added to a well (2 drops/ ml) and maintained at incubation of 20 minutes at 37°C, 90% humidity and 5% CO_2. After that, the slide was placed on the confocal microscope stage (Figure 2.1) and the subsequent imaging was performed using 40X water objective lens for high resolution imaging using the 405 nm laser. The microscope was maintained at 37°C, 90% humidity and 5% CO_2 during the imaging session. After choosing a suitable nucleus, the crop area was increased to visualize a single nucleus with detailed chromatin architecture. Once the nucleus was decided, an image was captured before adding the hydrogen peroxide. At this stage, the medium was pipetted out and medium containing H_2O_2 was added (with or without drug). Immediately after that step, the nucleus was found and imaged again. After that, images were captured every 5 minutes for 80 minutes. After that the Nucblue stain became very faint (because of photobleaching) and further imaging was not possible. For the same reason we performed the experiment with only 500 µM H_2O_2 treatment because all the drastic changes happened over 80 minutes, as discussed in the

results section. Additionally, the same experiment was performed at 20X magnification to visualize the response of MSC to oxidative stress at the population level, which was further quantified through the nuclear area change.

Quantification of nuclear area change

Before quantifying the chromatin remodeling, we assessed the response of the MSC at the population level through low resolution imaging (10X). The nucleus was visible through the Nucblue stain. This image channel was imported into the image processing software ImageJ. The nuclear area was detected by an edge tracking algorithm in ImageJ. Subsequently, the percentage of area change was calculated from the images pre H_2O_2 application and post H_2O_2 application.

Quantification of chromatin remodeling

After the live imaging was performed, the images were cropped and prepared ready for further postprocessing using ImageJ. A custom Matlab code was written for quantification of the chromatin remodeling index (CRI). The CRI was calculated at every timepoint with respect to the image corresponsing to the pre-H_2O_2 treatment. The images were registered using a series of Matlab function instructions. This step registered each pixel of the pre-H_2O_2 treatment image with the pixels of the post-H_2O_2 treatment timepoints. The result was a set of coordinates (X_t, Y_t) at every post-H_2O_2 treatment timepoint and initial coordinate (X_i, Y_i) of the pre-H_2O_2 treatment. Accordingly, CRI was calculated by using the following equation. Note that this quantity is in pixel which can be converted to micron if required.

$$CRI = [(X_t - X_i)^2 + (Y_t - Y_i)^2]^{1/2}$$

Before the Matlab code was applied, a drift correction algorithm was applied to the image stack using ImageJ to account for any bulk drifting of the nucleus. Therefore, the CRI only accounted for the real chromatin motion, and discarded any other movement of the bulk nucleus. Further,

chromatin condensation parameter (CCP) was calculated using a previously established technique published elsewhere (66). The Matlab code for this calculation is applied on a single image and it calculates how condensed the chromatin structure is in that image. The higher the number is, the chromatin is more compacted.

Segregation of chromatin domains

This step was performed based on a previously published work (67). Example of the procedure for a nucleus is shown in Figure 2.11. The pixels of the raw image are sorted based on the grayscale pixel intensity, which can have any integer value between 0 and 255, where 0 is absolute black and 255 is absolute white. The sorted pixels are represented in the blue solid curve in the plot. Hill function fits the blue solid curve with an appropriate mathematical equation, represented by the red dotted curve. The inflexion point in the red dotted curve represents a cut-off pixel intensity. Any pixel intensity higher than the cut-off intensity value is assigned to the heterochromatin domain, and any pixel intensity lower than this cut-off intensity value is assigned to the euchromatin domain. The technique was further modified to segregate the interchromatin region as well which is explained in Figure 2.16.

Statistics

All statistical difference calculation was performed using students' t-test between two groups (unpaired, heteroscedastic, two-tailed), and p value is reported in the results. All bar graphs display the mean with standard deviation about mean.

Table 2.1: List of key resources

REAGENT	SOURCE	IDENTIFIER
Experimental model: cell		
Mesenchymal Stem Cell	Lonza human bone marrow derived MSC	PT-2501
Reagents		
Cell culture medium	Lonza MSC medium bulletkit	PT-3001
Trypsin/ EDTA	Thermo Fisher	R-001100
DPBS, 1X	Corning	21-031-CV
PBS, pH7.4, 10X	Gibco	70011-044
NucBlue	Thermo Fisher	R37605
Cell viability assay: Live/dead viability kit	Thermo Fisher	L3224
Hydrogen Peroxide	Sigma Aldrich	216763
CellROX Green	Thermo Fisher	C10444
GSK126	Sigma	5005800001
Software for image analysis		
ImageJ	NIH	
Matlab	Mathworks	
Microscope		
Zeiss LSM 980 microscope	Zeiss	LSM 980 microscope

2.3 RESULTS

ARID1A inhibition decreases cell proliferation

In order to investigate how the GSK126, the ARID1A inhibitor affects the MSC, we investigated the bright field images of the cells. This experiment was required because no literature exists to understand the MSC behavior under GSK126, and therefore no baseline existed for us for the purpose of any comparison. As evident from Figure 2.2, the number of MSC were lower in GSK126 treated groups indicating the lower cell proliferation when ARID1A is inhibited. Interestingly, the cell phenotype was not visually different in control vs GSK126 treated groups. The MSC showed characteristic spindle like shape in both cases. Therefore, this data suggests that MSC viability and visual phenotype was maintained at the 20 μM concentration of GSK126.

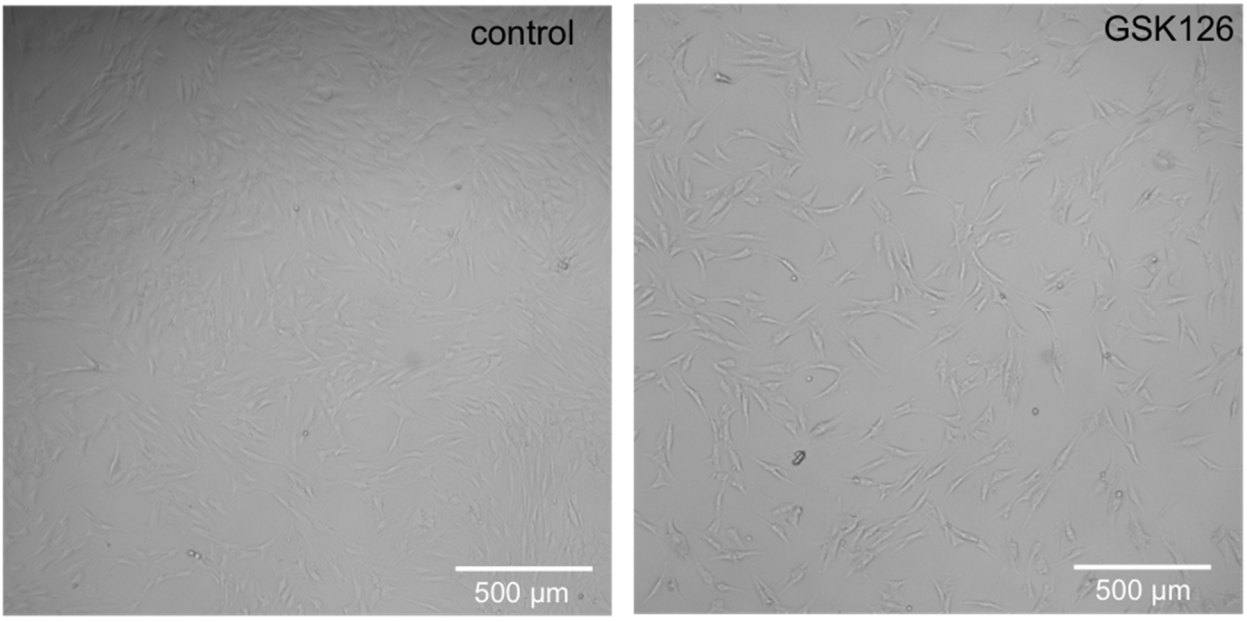

Figure 2.2 Number of cells were decreased in wells treated with GSK126, but the MSC phenotype was not distinctly different in the control vs GSK126 treated cases.

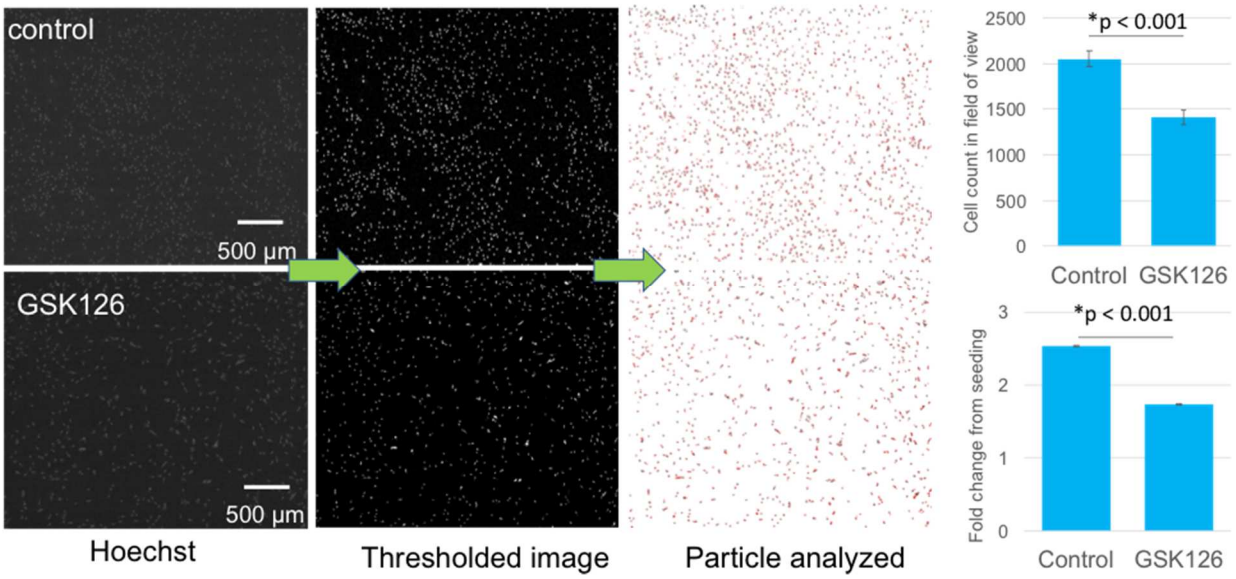

Figure 2.3 NucBlue staining and further imaging reveals that number of MSC post GSK126 treatment is lower, as quantitatively determines. (n = 8 field of views from 8 wells of each group)

Because the bright field images were not suitable for cell counting, NucBlue treated cells were used to count the cells. As evident from Figure 2.3, the number of cells were significantly lower in the GSK126 treated wells. When we calculated the fold change of the cells from the seeding it was further clear that the MSC proliferation was hindered in the GSK126 treated wells, characterized by almost 25% decrease in cell proliferation. This is expected because cell division requires the chromatin condensation at the interphase and that process requires extensive chromatin remodeling by the chromatin remodeling complex. ARID1A inhibition should affect the process of chromatin condensation and therefore, the MSC proliferation was hindered.

ARID1A inhibition does not affect the cell viability

We applied 20 µM GSK126 and the cell phenotype indicated that the cells were healthy. However, to further confirm if the ARID1A inhibition causes any cell death or not, we checked the number of live cells vs dead cells in both groups. First, we validated the concentration of the live/ dead assay by controlled killing and calcein AM/ Ethidium homodimer -1 treatment of

staining of cells. Figure 2.4 reveals that the viability assay with our chosen and optimized concentration indeed works with the MSC. Left column of Figure 2.5 reveals that the GSK126 treatment does not significantly lower the cell viability. In fact, the number of dead cells were very few in both cases which not only shows that ARID1A inhibition does not affect the cell viability but also it is a testament to our high quality and sterile cell culture practice. We quantified the data further, as shown in the bar graph in Figure 2.5. The viability of control (- H_2O_2, -GSK126) and GSK126 treatment groups (- H_2O_2, +GSK126) remained at 93%-95%. This set of data provided us with the confidence to move on to study the effect of hydrogen peroxide in the chromatin remodeling. As a note, we used the concentration of 20 µM GSK126 from the literature, as other studies used that concentration in MSC (68).

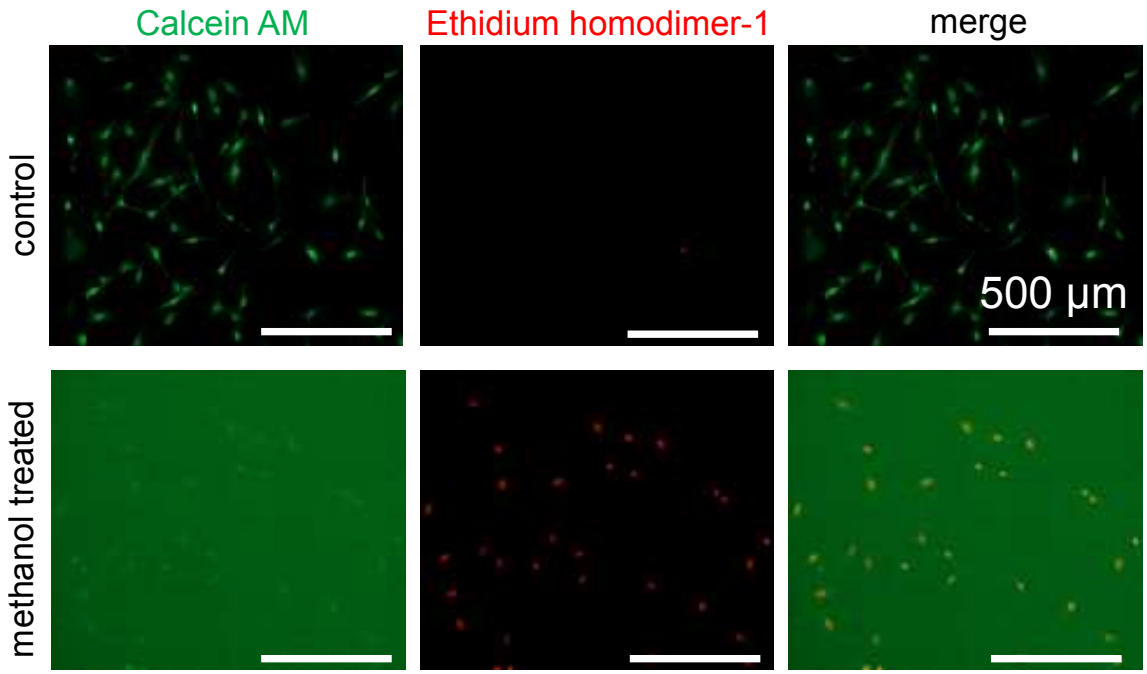

Figure 2.4 Live/ dead cell viability assay was validated by exposing the MSC to 70% methanol for 30 minutes, thus completely killing the cells. Red (dead) nuclei are visible in the methanol treated group. Such dead nuclei are almost non-existent in the control group. Data reported based on 4 technical replicates.

Interestingly, as evident from Figure 2.5, on the exposure of hydrogen peroxide to the non GSK126 treated group, (+ H_2O_2, -GSK126), the cell viability also did not decrease compared to the control group (- H_2O_2, -GSK126), it remained at around 93%. However, on the exposure of hydrogen peroxide to the non GSK126 treated group, (+ H_2O_2, -GSK126), the MS viability dropped to 82% which confirms a functional role of ARID1A in MSC survival post oxidative stress.

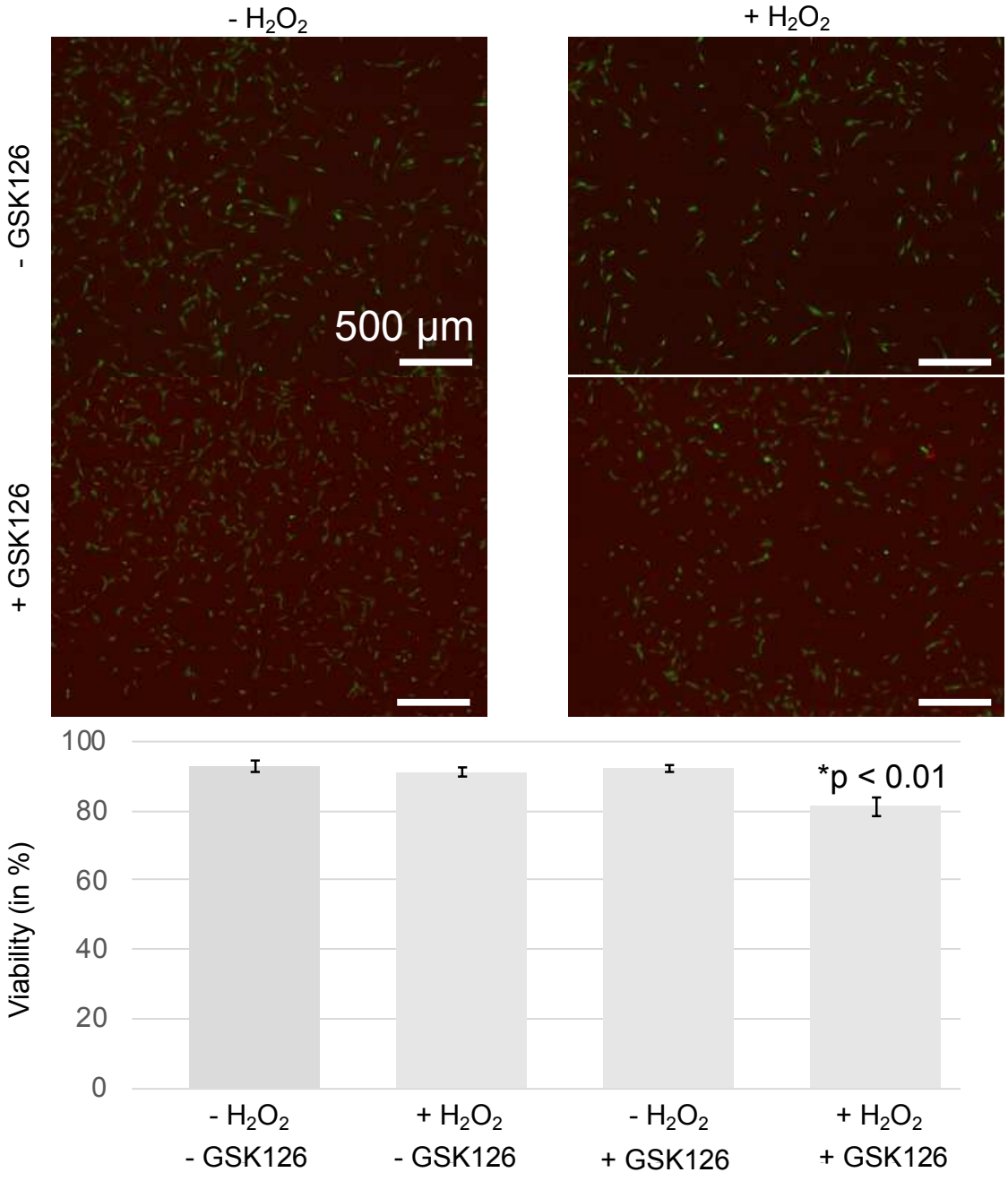

Figure 2.5 Live/ dead cell viability assay reveals that the viability of MSC post GSK126 treatment is not compromised. Further, H_2O_2 exposure does not compromise the MSC viability but GSK126 treatment of MSC before the H_2O_2 exposure decreases the MSC viability thus confirming a functional requirement of ARID1A in MSC upon the oxidative stress. Data reported based on 4 technical replicates.

Hydrogen peroxide treatment cause ROS generation

Next, we validated the generation of ROS under the hydrogen peroxide treatment. Figure 2.6 reveals that hydrogen peroxide treatment indeed increases the generation of ROS, as shown by the enhanced green color at higher concentration of hydrogen peroxide. Although these studies were at lower concentration, our 500 µM hydrogen peroxide was poised to increase the ROS.

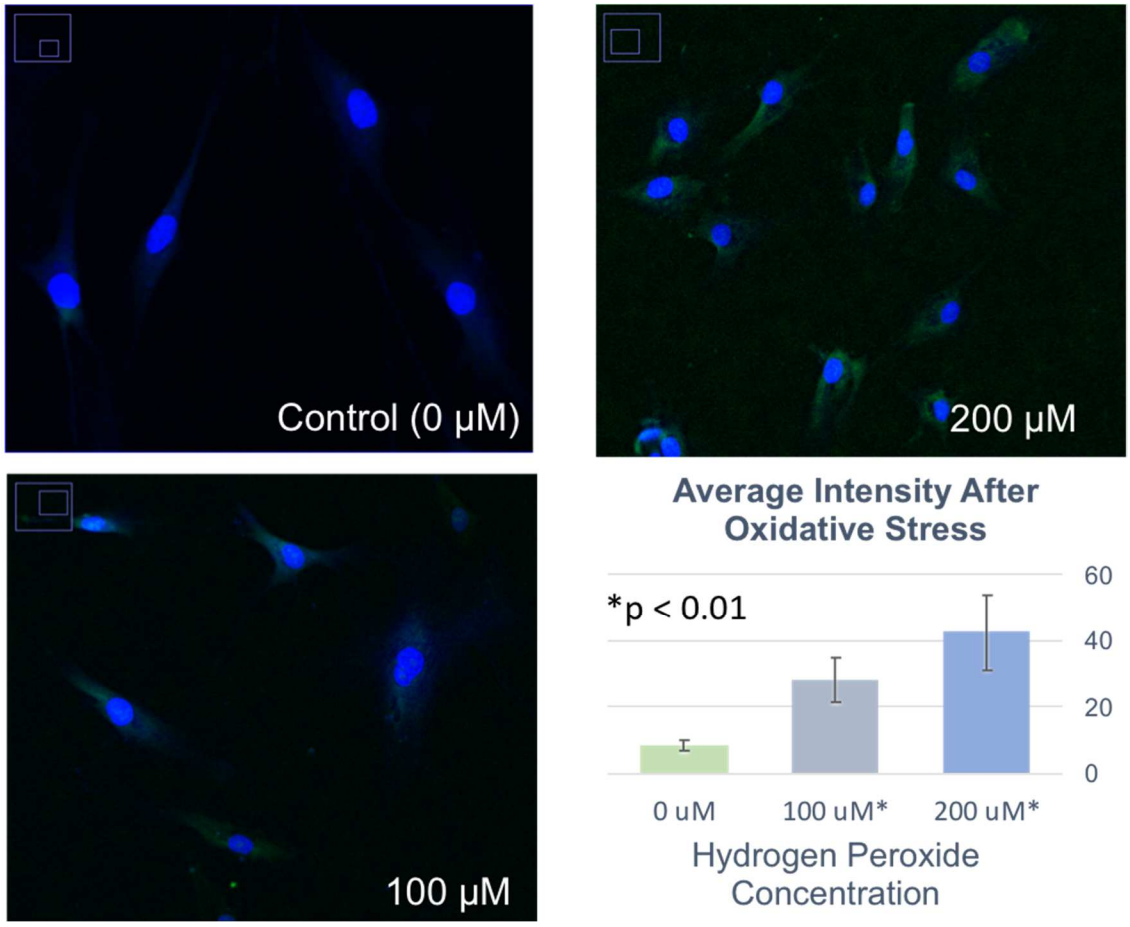

Figure 2.6 CELLROX staining and imaging confirms that hydrogen peroxide treatment indeed increases the ROS generation as quantified by the image average image intensity of the green channel. Number of field of views = 3, based on three different wells.

Nuclear area shrinkage is caused by hydrogen peroxide which is dampened by ARID1A inhibition by GSK126

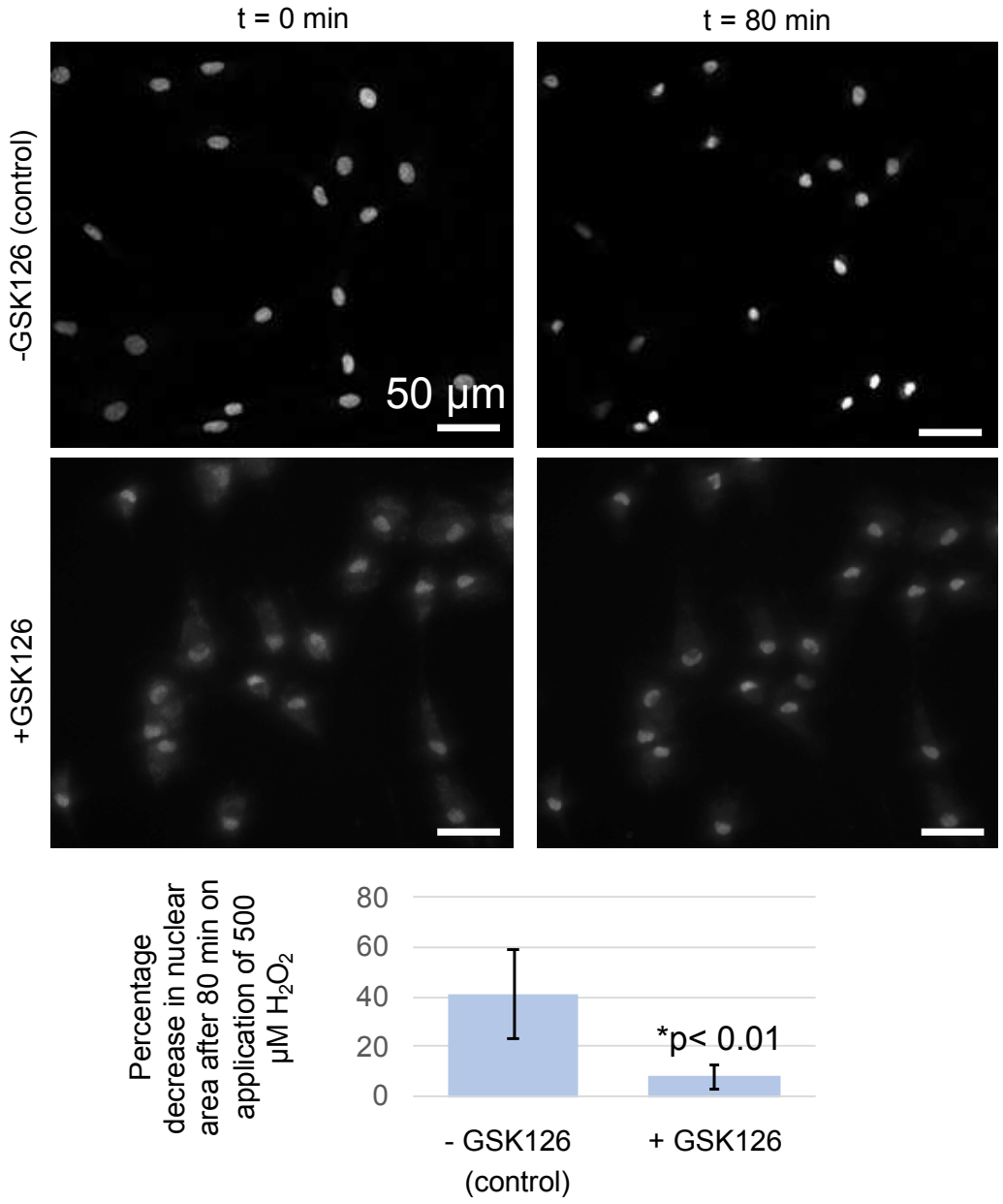

Figure 2.7 On the application of 500 µM H_2O_2, the MSC nuclei shrinks. GSK126 which inhibits the chromatin remodeling by blocking ARID1A, ameliorates such shrinkage. Data based upon 5 technical replicates with at least 50 nuclei from each group.

Figure 2.7 reveals that hydrogen peroxide treatment causes shrinkage of the nucleus by almost 40%. The shrinkage is significantly lowered (to ~8%) by the GSK126 treatment of the MSC. Combining the results from Figure 2.5 and Figure 2.7 we can conclude that the ARID1A is required for the nucleus shrinkage for maintaining the MSC viability upon the exposure of hydrogen peroxide. Based on this data of bulk nuclear area change, we executed the high-resolution quantification of intranuclear changes upon hydrogen peroxide treatment, as described in the next section.

Rapid chromatin remodeling under hydrogen peroxide is dampened by ARID1A inhibition

After we were confident about the cell culture system, imaging system, GSK126 treatment, hydrogen peroxide treatment, cell viability and the nuclear area shrinkage upon hydrogen peroxide, we performed the live imaging and analysis of intranuclear space in high spatiotemporal details. The live imaging revealed that at the onset of hydrogen peroxide treatment, in the control group the chromatin gradually remodels. The effect is initially evident at the nuclear periphery but eventually the nuclear interior remodels drastically after 15-20 minutes and the remodeling continues to increase until it stabilizes at around 50 minutes and persists for a longer time until the end of our imaging session. The timepoints reported in the previous sentence is for a representative nucleus only. The details of the remodeling map is quantified through the chromatin remodeling index (CRI) and is shown in Figure 2.8 for the representative nucleus. Please note that for each nucleus that timepoint was slightly different, but the effect of high chromatin remodeling was evident. On the contrary, the GSK126 treatment drastically reduced the hydrogen peroxide mediated chromatin remodeling as revealed through the image sequence and CRI map presented in Figure 2.9 for a representative nucleus. There was some remodeling in those nuclei, but the effect was much lower compared to the non-treated control nucleus. This data indicates that

ARID1A inhibition impairs the chromatin remodeling process. For Figure 2.8 and 2.9, the image maps were obtained for 80 minutes and 70 minutes respectively. The imaging setting was maintained at the lower end of the laser power (0.5% in the 405 nm) and increased up to 0.8% during the imaging if required, because photobleaching gradually decreased the image intensity. After 70 – 80 minutes photobleaching was unavoidable and the imaging was stopped. Interestingly, most chromatin remodeling happened within this timeframe. Of 70-80 minutes and further events may not be critical for imaging and further documentation.

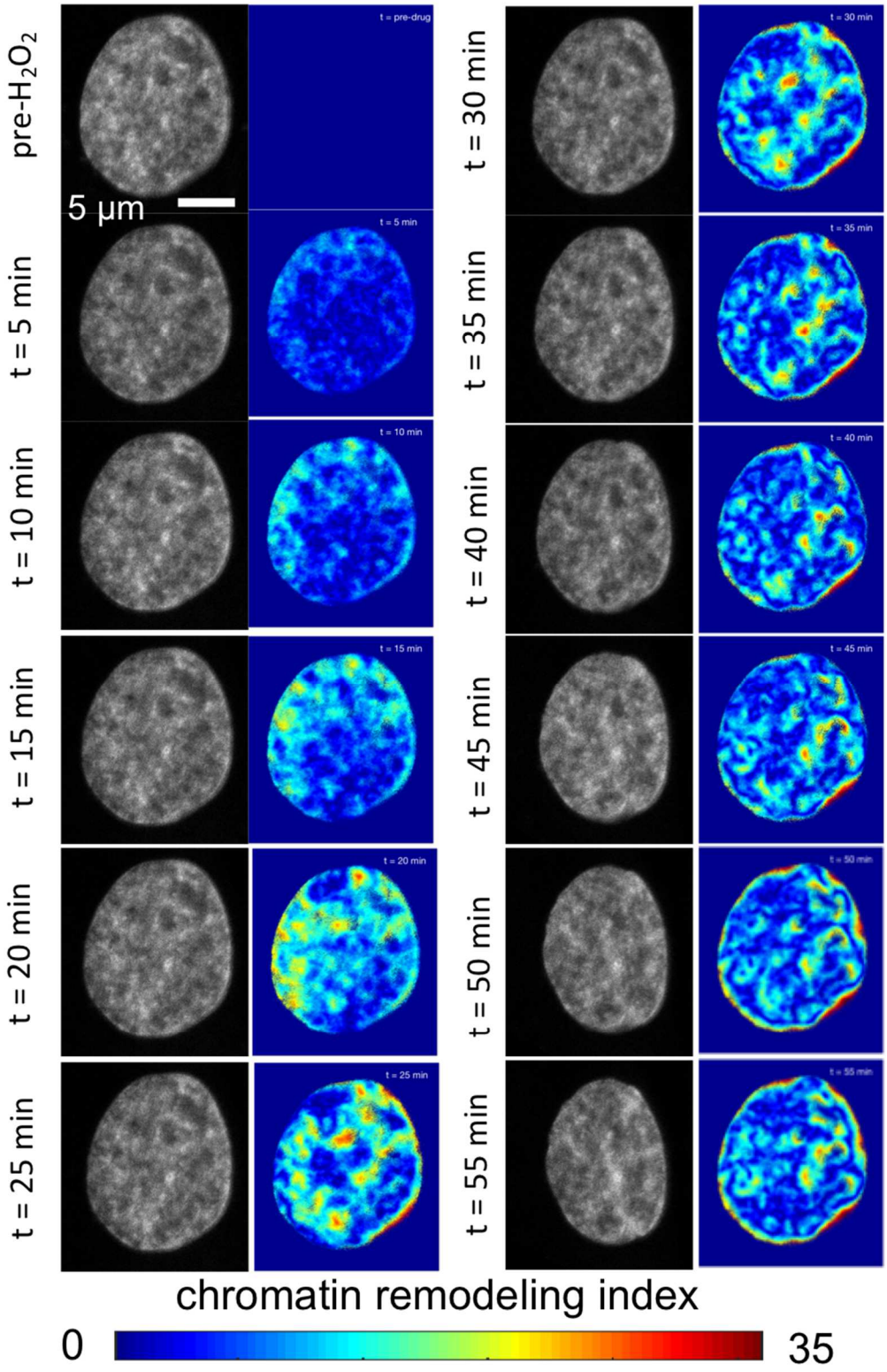

Figure 2.8 Time lapse image sequence of a nucleus and chromatin remodeling index map for a representative nucleus without GSK126 treatment (control).

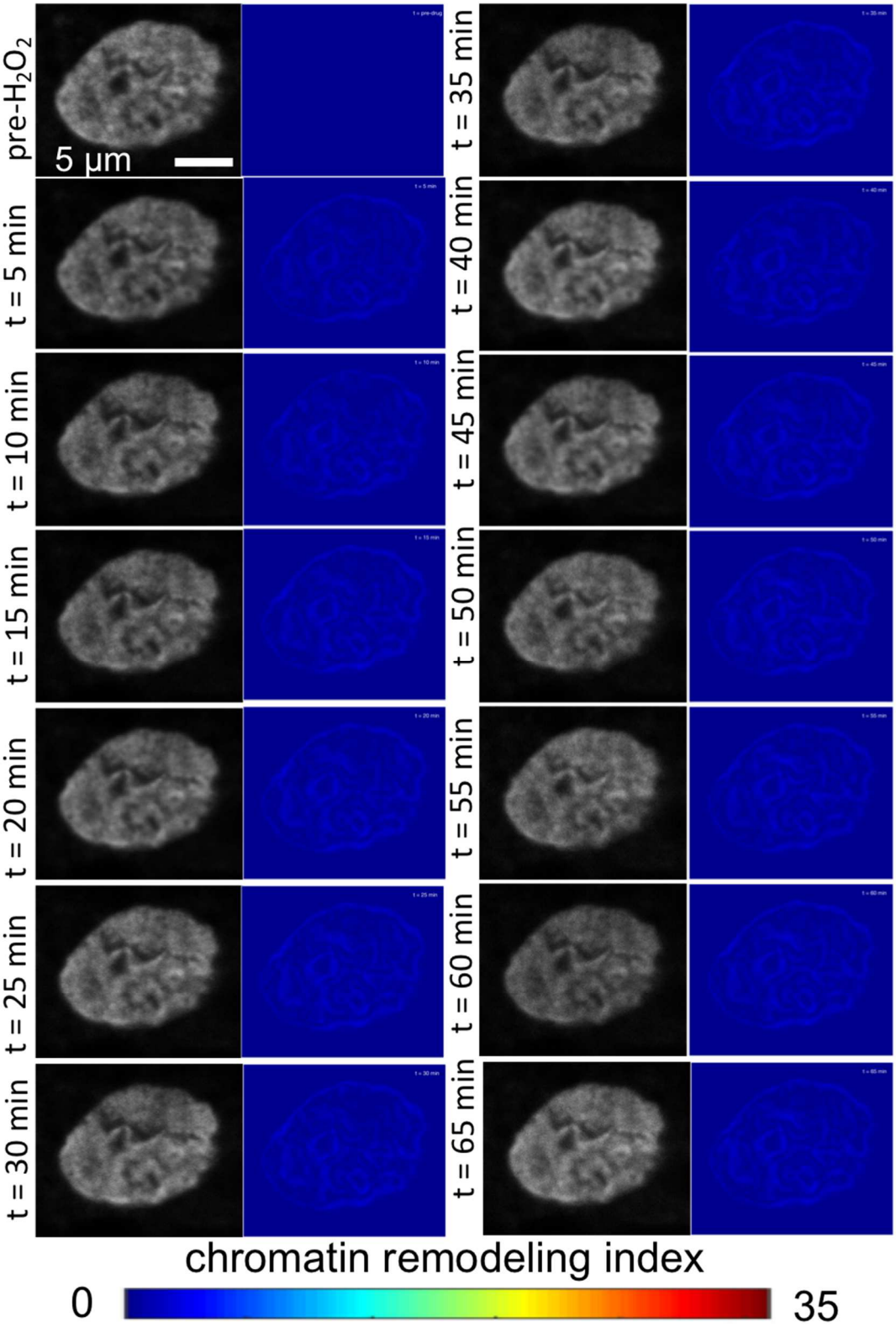

Figure 2.9 Time lapse image sequence of a nucleus and chromatin remodeling index map for a representative nucleus with GSK126 treatment.

To obtain a robust quantitative measure of CRI for the comparison purpose between the two groups: non-treated vs GSK126 treated, the average CRI over the entire nucleus at the mid timepoint of t = 35 or 40 min was used (Figure 2.10), depending on the total imaging time of 70 min or 80 min. The nucleus-averaged CRI was significantly higher for the control group at the mean value of 8, compared to the GSK126 treated group which has a mean value of around 1.6. This observation generally matches the CRI map of the entire nucleus as shown in Figure 2.8 and Figure 2.9. Although we found higher values of CRI in many nuclear locations in the control group, overall, the average value was lower than expected because many locations of the nucleus experienced a lower CRI value at the mid timepoint. Further, the chromatin condensation parameter (CCP) was used to quantify the end CCP magnitude compared to starting (pre-hydrogen peroxide) CCP. That quantity is also significantly changed in control group (Figure 2.10) whereas for the GSK126 treated group, the CCP does not change before the hydrogen peroxide treatment and at the end of the remodeling. Together, this data supports our hypothesis that ARID1A is an important component, required for chromatin remodeling.

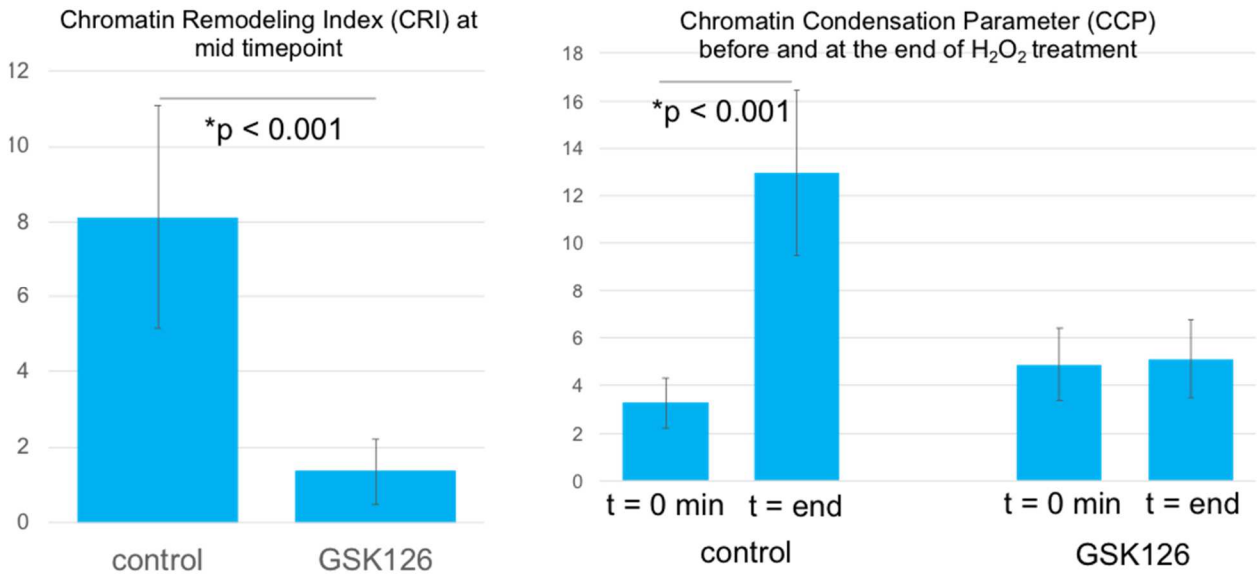

Figure 2.10 Both CRI and CCP quantification shows that GSK126 treatment hinders the chromatin remodeling (n = 5 nuclei from each group). For the CCP values, t = end means either 70 min or 80 min depending on the length of the imaging session.

Spatiotemporal chromatin remodeling pattern inside the nucleus is complex

Next, we wanted to further understand how the evolution of CRI looks like in different nuclear regions in a spatiotemporal manner. We looked into regions such as nuclear periphery vs nuclear interior. Also, we wanted to understand if any difference of CRI evolution exists between the euchromatin and the heterochromatin regions in terms of the maximum CRI values at a given location. For faithfully assigning the different regions of nucleus to euchromatin and heterochromatin regions, we used a technique that we developed before (67) and a segregated nucleus using this method is shown in Figure 2.11.

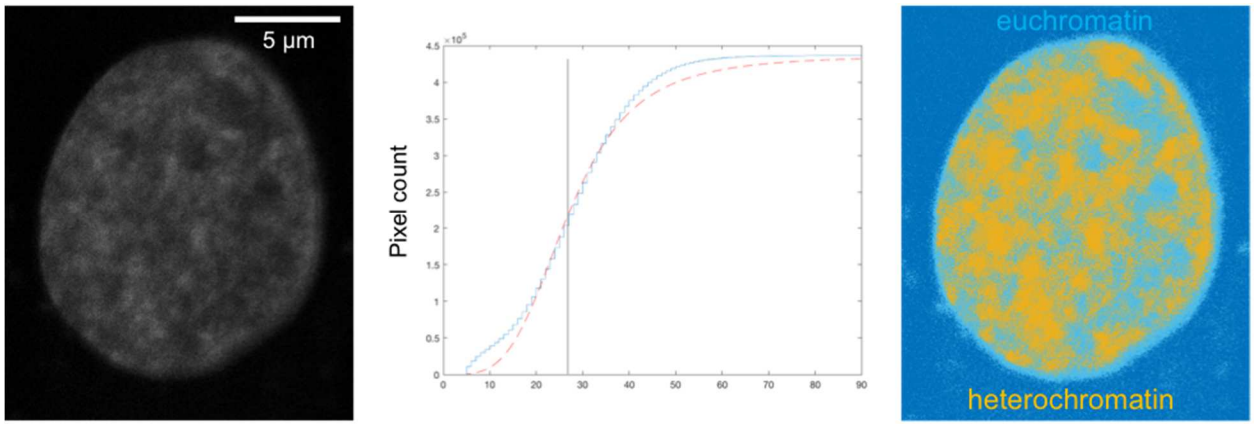

Figure 2.11 Segregated nucleus with euchromatin and heterochromatin. The S-curve at the middle is generated to have an automated segregation algorithm of the chromatin image intensity values.

The time lapse CRI plots of several points (at euchromatin vs heterochromatin, and also at nuclear periphery vs interior) is shown in Figure 2.12 (euchromatin) and Figure 2.13 (heterochromatin). We found that points at the peripheral areas experience higher CRI earlier whereas the interior points experience higher CRI later as seen for points 4 and 6 in Figure 2.12.

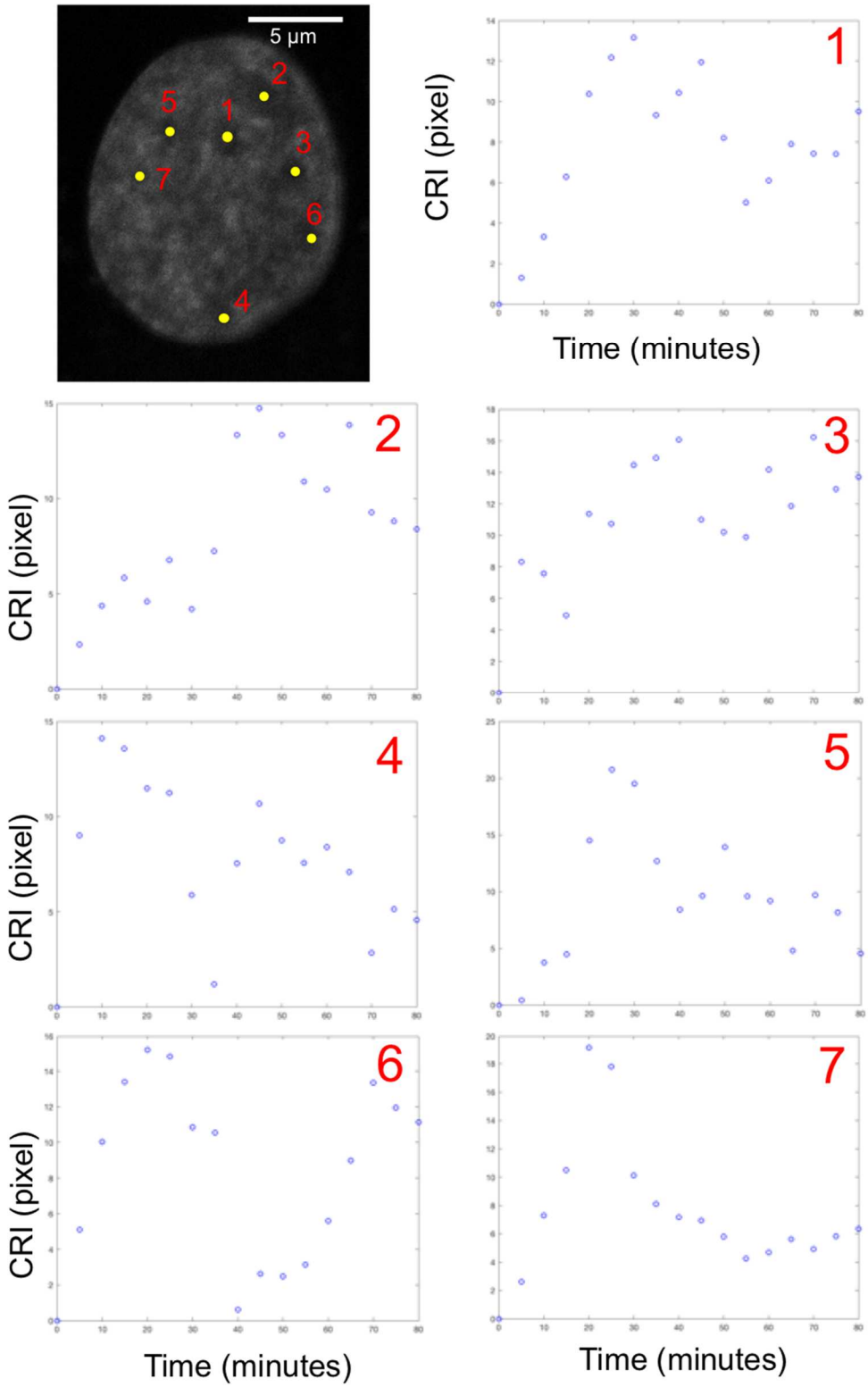

Figure 2.12 Time lapse CRI values for sample points in the nucleus, all points pertain to euchromatin. Some points experience the CRI early, and some points experience CRI later.

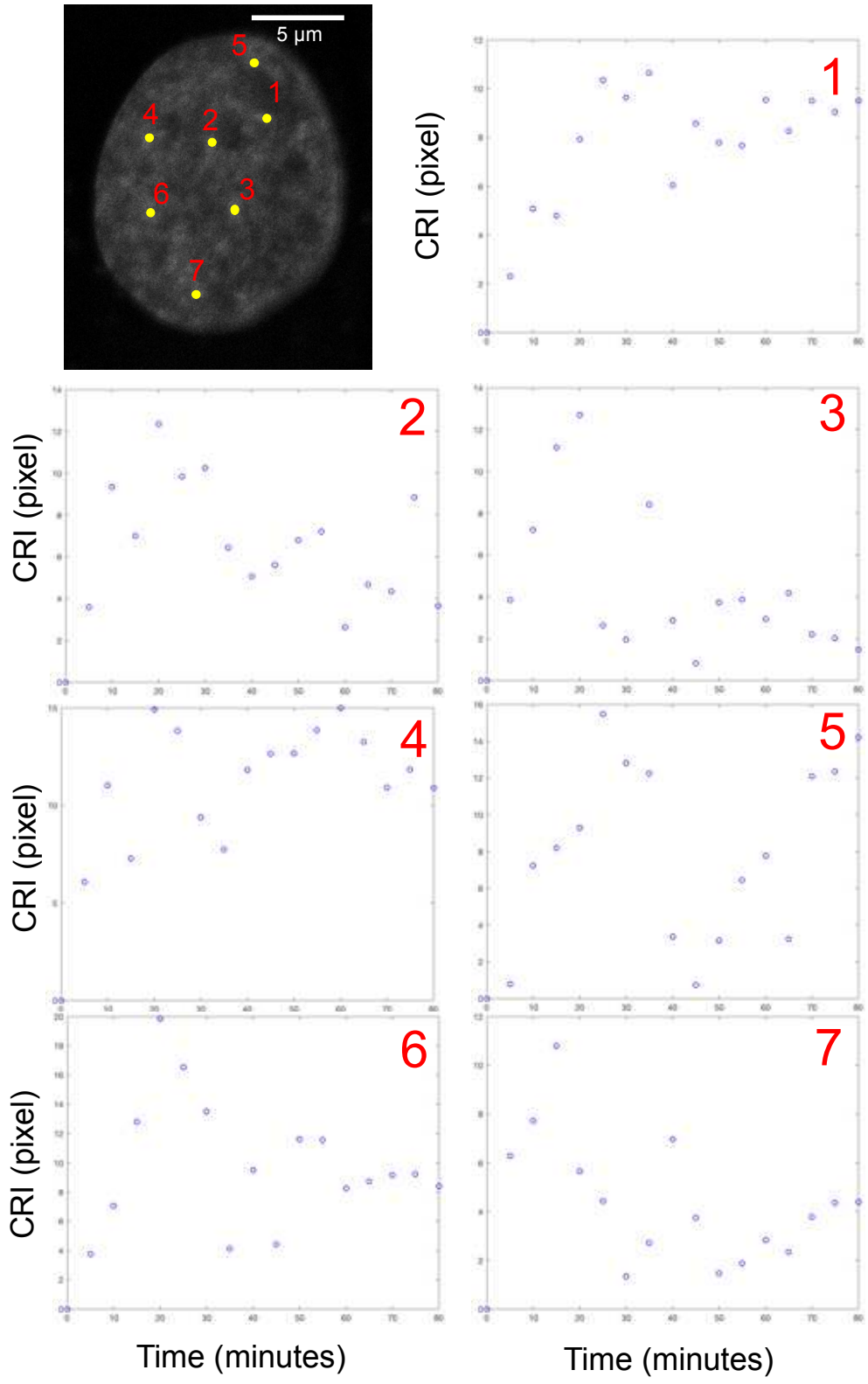

Figure 2.13 Time lapse CRI values for sample points in the nucleus, all points pertain to euchromatin. Some points experience the CRI early, and some points experience CRI later.

Overall, the results presented in Figure 2.12 and Figure 2.13 reveals that the CRI is experienced in both regions of the heterochromatin and euchromatin, and not preferentially in one specific region, and the map is complex. However, when we looked into the CRI map and compared the values at the segregated euchromatin and heterochromatin regions, we found that both regions indeed experience high CRI but at a given timepoint (t = 25 min for example), the heterochromatin generally has the high CRI hotspots (Figure 2.14). However, we found that the area averaged heterochromatin CRI value (CRI = 15.55 ± 5.81) was not significantly higher (*p= 0.35) compared to the area averaged euchromatin CRI value (CRI = 12.71 ± 3.19) at the mid time point (t = 40 min or 35 min) based on 5 nuclei.

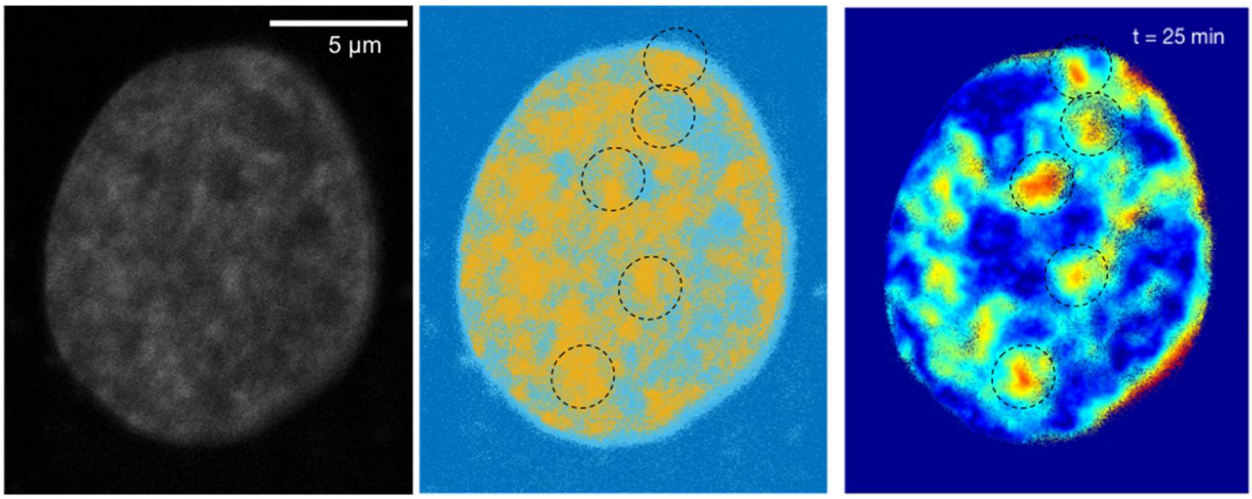

Figure 2.14 Although both euchromatin and heterochromatin regions experience high and low chromatin remodeling, hotspots exist mostly at the heterochromatin regions (marked by the dotted circles in the middle figure panel).

It is apparent from the Figure 2.12 and Figure 2.13 that some points in the nucleus experience high CRI but eventually lowers to a smaller value over time when the chromatin remodel slows down. Both heterochromatin and euchromatin regions contain such points. However, some points persist a higher chromatin value at the end timepoint – such as points 1 and 5 in Figure 2.12. Very interestingly, when we looked into the final CRI map at t = 80 min (Figure

2.15), we found that the most persistent CRI occurs at the heterochromatin-euchromatin interface. This is not only true for highly remodeled control group nucleus chromatin, but also for GSK126 treated nucleus. The fact that the CRI is most persistent at these locations indicate that the heterochromatin-euchromatin conversion or vice versa might be possible at these interfacial locations as the long-term effect. Heterochromatin-euchromatin interface (interchromatin) has been previously proposed (69) to be a hub of most chromatin remodeling activity in multiple contexts, and for the first time our data visualize and quantify this phenomenon. To confirm this phenomenon, we further analyzed the data of CRI at t = 80 min for heterochromatin, euchromatin and the interchromatin (Figure 2.16a). The area averaged value of CRI at the interchromatin region (Figure 2.16b) indeed confirms a persistent chromatin remodeling at that region compared to the heterochromatin and the euchromatin regions.

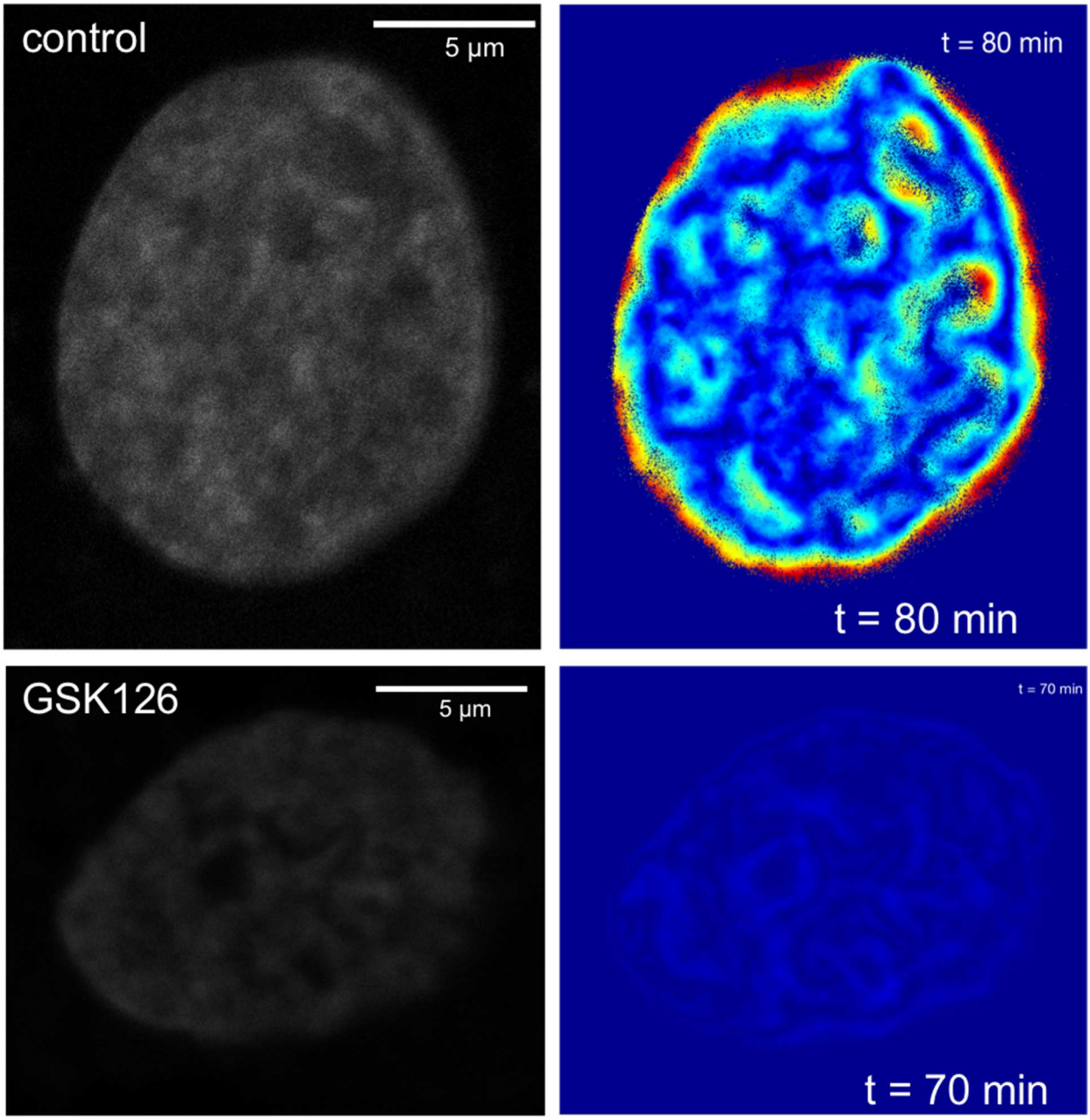

Figure 2.15 CRI is most persistent at the heterochromatin and euchromatin interface (interchromatin) as evident from the higher residual values of CRI at the end of the imaging session.

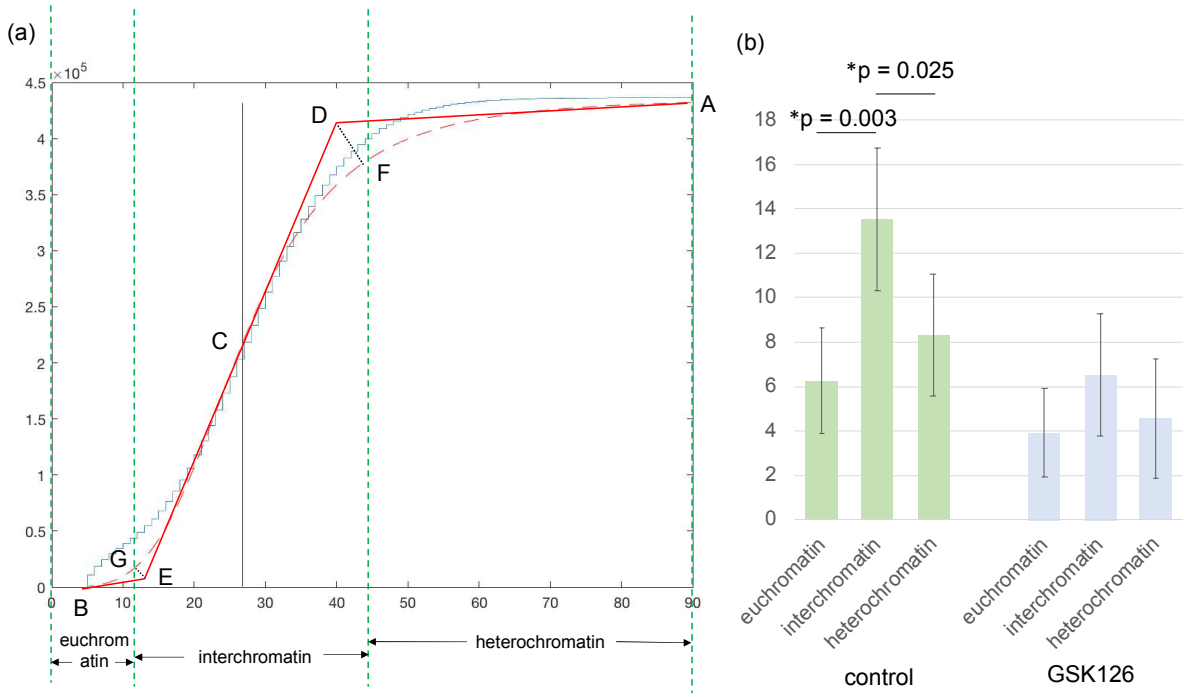

Figure 2.16 Interchromatin region was segregated from the euchromatin and the heterochromatin region using an automated algorithm. After sorting the pixels by pixel intensity, we find an 'S-curve'. The highest 50 pixel points are used for fitting a straight line AD. The 50 points around the inflexion point C is used to fit another line ED. AD and ED meets at point D. A normal is dropped from the point D on the S curve. That point F is designated as the cut-off between the interchromatin and heterochromatin. Similarly, a straight line (BE) is fit based upon the lowest 50 pixel points. The lines DE and BE meet at point E. A normal is dropped from the point E on the S curve which marks the point G. Point G is marks the cut-off between the euchromatin and interchromatin regions. Bar graph indicates that for non GSK126 treated group, the chromatin remodeling is persistent at t = 80 min at the interchromatin region.

2.4 DISCUSSION

Overall, this work creates a technical framework to visualize and quantify the chromatin remodeling in real time. Quantification of chromatin remodeling and understanding its functional significance is growing research niche. Such understanding is required to understand the response of cells towards DNA damage and to understand how the cells maintain genomic stability after experiencing environmental stress. This work is the first attempt to accomplish those technical abilities using a specific cell type, but the technique can be applied to many applications with other

cell types. Therefore, this work is innovative and timely given the ongoing efforts in the nuclear/ chromatin biology research community.

Our approach is based on robust image processing techniques, but further work is required to make the data processing workflow easier and to denoise the CRI maps. Advanced image processing and noise cancelling algorithm might be able to achieve that. The biggest limitation of this proof-of-concept work is the use of NucBlue (a live imaging formulation of Hoechst) which is easily photobleached even at a very low laser power. Therefore, Nucblue is not the best dye to image intranuclear architecture and its dynamics. Endogenous probes such as fluorescent H2B coding gene can be integrated to the chromatin for long-term imaging without the risk of photobleaching. With that modality of imaging, more ambitious questions can be answered such as how the chromatin compaction happens in 3D because using those probes, we can capture the full 3D volumetric map of the nucleus. In our work, the third dimension was very small, 2D representation of the CRI mapping is valid but 3D imaging with multiple images in the z stack will provide us with more insight into the CRI map.

MSC become senescent and do not perform optimally in aged people, and also, MSC extracted from aged population do not show the optimal expansion or regeneration ability(70, 71). Aging is inherently associated with oxidative stress characterized by the abundance of ROS in aged tissues(72). It is important to understand whether and how MSC combat the oxidative stress to achieve the most optimal translational output from MSC. This work not only points to the fact that MSC experiences chromatin remodeling under oxidative stress but also our work points to ARID1A as a key mediator of the chromatin remodeling, which is probably required to maintain the genomic stability in MSC. Moving forward, it is important to understand whether MSC from

aged individuals have lower ARID1A expression which will help us to identify and potentially intervene the mechanism of MSC performance in/ from aged individuals.

ARID1A was identified a key mediator of chromatin remodeling in this work. Although this is intriguing, we only used a drug at a certain concentration. The drug we used indirectly blocks the ARID1A through inhibition of EZHII, and this drug is one of the most commonly used drugs for ARID1A inhibition. In fact, this drug is used to treat cancer for several cancer phenotypes where a genetic mutation is associated with the gene encoding ARID1A(73). More direct blocking of ARID1A can be obtained through RNA interference strategy. It is not clear if ARID1A actually maintains the structural integrity of the chromatin or is actively engaged in the chromatin remodeling. Blocking multiple molecules in the SWI/ SNF complex might answer those questions. Moreover, the functional meaning of chromatin remodeling was not revealed in this study. Thorough quantification of DNA damaging markers in the presence and absence of GSK126 can only reveal what is the functional significance of such stress induced chromatin remodeling or the lack of it.

The hydrogen peroxide treatment we used is very high – 500 μM, which is much higher than the physiological ROS level, although 500 μM has been used in multiple previous studies. The experiments need to be performed at lower concentration of hydrogen peroxide. In our preliminary study we tried a lower concentration and the chromatin remodeling still happened at a lower concentration. But the chromatin remodeling was relatively slow under those conditions and long-term imaging was difficult because of photobleaching. Endogenous fluorescent H2B markers in the chromatin can potentially ease that limitation.

We found that ARID1A inhibition causes lower viability of MSC under hydrogen peroxide treatment. Although this can be viewed as an immediate functional meaning of MSC related to

survival, whether ARID1A also plays a role in regenerative function of MSC after oxidative stress is not addressed in this study. To achieve that, we need to design experiments to use the viable MSC after the oxidative stress treatment and assess the MSC specific marker (growth factors). Besides, the present study does not address the detailed mechanism of how the ARID1A actually helps in the chromatin remodeling and how it contains the DNA damage. Experiments with endogenous H2B markers (which are resistant to photobleaching) and DNA damage markers can answer the question.

Finally, interfacial phenomenon at the heterochromatin-euchromatin boundary is an emerging area of study. Observation of persistent chromatin remodeling at those locations is intriguing but we do not know whether this phenomenon is biophysical or biochemical, and what is the functional meaning of such persistent remodeling. Further studies are required to discover any interesting mechanism that might be underlying such observation. Such study might include the endogenous fluorescent tagging of remodeling markers.

CHAPTER 3

CONCLUSIONS AND FUTURE WORK

This work builds the technical and conceptual framework of multiple future projects. A few are listed below.

(1) The different subunits of SWI/SNF complex can be differentially inhibited to understand the role of different components of SWI/SNF in chromatin remodeling. This work will be enhanced and potentially benefitted by the collaboration with structural biologists.

(2) Endogenous H2B fluorescent marker will open the avenue for long term imaging and understanding the chromatin remodeling under physiological oxidative stress conditions.

(3) The technical framework is valid for any cell type and is suitable for studying the chromatin remodeling under other stresses such as toxin and UV light.

(4) Some endpoint DNA damage assays can be attempted. For example, it will be interesting to visualize if the DNA damage and repair marker intensity and distribution of γ-H2AX, 53BP1 or Rad50 are changed by ARID1A inhibition. Such immunofluorescence assay can be performed in the shorter term.

(5) A very interesting study will be to visualize the DNA damage live using a fluorescent protein, and also to visualize the chromatin remodeling using another color of fluorescent protein such as H2B. Such study will reveal in real time how, when and where the chromatin remodeling happens post-stress to repair the nucleus and hence, to maintain the chromatin integrity.

LIST OF REFERENCES

1. Isermann, P., and J. Lammerding. 2013. Nuclear mechanics and mechanotransduction in health and disease. *Current Biology*. 23:R1113–R1121.
2. 2007. Nuclear Dynamics. Springer International.
3. 2011. The Nucleus. Cold Spring Harbor Laboratory Press.
4. Pombo, A., and N. Dillon. 2015. Three-dimensional genome architecture : players and mechanisms. *Nature Reviews Molecular Cell Biology*. 16:245–257.
5. Baumann, K. 2017. A vision of 3D chromatin organization. *Nature Reviews Molecular Cell Biology*. 18:532.
6. Li, G., and D. Reinberg. 2011. Chromatin higher-order structures and gene regulation. *Current Opinion in Genetics & Development*. 21:175–186.
7. Woodcock, C.L., and R.P. Ghosh. 2010. Chromatin higher-order structure and dynamics. *Cold Spring Harbor Perspectives in Biology*. 2:a000596.
8. Chen, Z., S. Li, S. Subramaniam, J.Y.J. Shyy, and S. Chien. 2017. Epigenetic regulation : A new frontier for biomedical engineers. *Annual Review of Biomedical Engineering*. 19:195–219.
9. 2015. Epigenetics. 2nd ed. Cold Spring Harbor Laboratory Press.
10. Ghosh, S., V.C. Cuevas, B. Seelbinder, and C.P. Neu. 2020. Image-based elastography of heterochromatin and euchromatin domains in the deforming cell nucleus. *bioRxiv*.
11. Grewal, S.I.S., and S. Jia. 2007. Heterochromatin revisited. *Nature Reviews Genetics*. 8:35–46.
12. Richards, E.J., and S.C.R. Elgin. 2002. Epigenetic codes for heterochromatin formation and silencing: rounding up the usual suspects. *Cell*. 108:489–500.

13. Damodaran, K., S. Venkatachalapathy, F. Alisafaei, A. V. Radhakrishnan, D.S. Jokhun, V.B. Shenoy, and G. V. Shivashankar. 2018. Compressive force induces reversible chromatin condensation and cell geometry–dependent transcriptional response. *Molecular Biology of the Cell*. 29:3039–3051.

14. Clapier, C.R., J. Iwasa, B.R. Cairns, and C.L. Peterson. 2017. Mechanisms of action and regulation of ATP-dependent chromatin-remodelling complexes. *Nature Reviews Molecular Cell Biology*. 18:407–422.

15. Längst, G., and L. Manelyte. 2015. Chromatin remodelers: from function to dysfunction. *Genes*. 6:299–324.

16. Saha, A., J. Wittmeyer, and B.R. Cairns. 2006. Chromatin remodelling : the industrial revolution of DNA around histones. *Nature reviews Molecular Cell Biology*. 7:437–447.

17. Lorch, Y., B. Maier-Davis, and R.D. Kornberg. 2010. Mechanism of chromatin remodeling. *Proceedings of the National Academy of Sciences of the United States of America*. 107:3458–3462.

18. Reyes, J.C., C. Muchardt, and M. Yaniv. 1997. Components of the human SWI/SNF complex are enriched in active chromatin and are associated with the nuclear matrix. *Journal of Cell Biology*. 137:263–274.

19. Euskirchen, G., R.K. Auerbach, and M. Snyder. 2012. SWI/SNF chromatin-remodeling factors : multiscale analyses and diverse functions. *Journal of Biological Chemistry*. 287:30897–30905.

20. Toto, P.C., P.L. Puri, and S. Albini. 2016. SWI/SNF-directed stem cell lineage specification: dynamic composition regulates specific stages of skeletal myogenesis. *Cellular and Molecular Life Sciences*. 73:3887–3896.

21. Alfert, A., N. Moreno, and K. Kerl. 2019. The BAF complex in development and disease. *Epigenetics & Chromatin*. 12:1–15.

22. Mani, U., A.S. Sankareswaran, A.R.N. Goutham, and S.M. Mohan. 2017. SWI / SNF Infobase - An exclusive information portal for SWI / SNF remodeling complex subunits. *PLoS ONE*. 12:1–11.

23. Alver, B.H., K.H. Kim, P. Lu, X. Wang, H.E. Manchester, W. Wang, J.R. Haswell, P.J. Park, and C.W.M. Roberts. 2017. The SWI/SNF chromatin remodelling complex is required for maintenance of lineage specific enhancers. *Nature Communications*. 8:1–10.

24. Bevilacqua, A., M.S. Willis, and S.J. Bultman. 2014. SWI / SNF chromatin-remodeling complexes in cardiovascular development and disease. *Cardiovascular Pathology*. 23:85–91.

25. Dutta, A., M. Sardiu, M. Gogol, J. Gilmore, D. Zhang, L. Florens, S.M. Abmayr, M.P. Washburn, and J.L. Workman. 2018. Composition and function of mutant SWI/SNF complexes. *Cell Reports*. 18:2124–2134.

26. Nguyen, H., G. Sokpor, L. Pham, J. Rosenbusch, A. Stoykova, J.F. Staiger, and T. Tuoc. 2016. Epigenetic regulation by BAF (mSWI/SNF) chromatin remodeling complexes is indispensable for embryonic development. *Cell Cycle*. 15:1317–1324.

27. Hadidy, N.E., and V.N. Uversky. 2019. Intrinsic disorder of the BAF complex : roles in chromatin remodeling and disease development. *International Journal of Molecular Sciences*. 20:1–59.

28. Kadoch, C., and G.R. Crabtree. 2015. Mammalian SWI / SNF chromatin remodeling complexes and cancer : mechanistic insights gained from human genomics. *Science Advances*. 1:1–18.

29. Romero, O.A., and M. Sanchez-Cespedes. 2014. The SWI / SNF genetic blockade : effects in cell differentiation, cancer and developmental diseases. *Oncogene*. 33:2681–2689.

30. Mittal, P., and C.W.M. Roberts. 2020. The SWI/SNF complex in cancer - biology, biomarkers and therapy. *Nature Reviews Clinical Oncology*. 17:435–448.

31. Masliah-Planchon, J., I. Bieche, J.M. Guinebretière, F. Bourdeaut, and O. Delattre. 2015. SWI / SNF chromatin remodeling and human malignancies. *Annual Review of Pathology: Mechanisms of Disease*. 10:145–171.

32. Prasad, P., A. Lennartsson, and K. Ekwall. 2015. The roles of SNF2/SWI2 nucleosome remodeling enzymes in blood cell differentiation and leukemia. *BioMed Research International*. 15:1–17.

33. Tower, J. 2012. Stress and stem cells. *Wiley Interdiscip Rev Dev Biol*. 1:1–18.

34. Spees, J.L., R.H. Lee, and C.A. Gregory. 2016. Mechanisms of mesenchymal stem/stromal cell function. *Stem Cell Research and Therapy*. 7.

35. Raheja, L.F., D.C. Genetos, A. Wong, and C.E. Yellowley. 2011. Hypoxic regulation of mesenchymal stem cell migration: The role of RhoA and HIF-1α. *Cell Biology International*. 35.

36. Toupadakis, C.A., J.L. Granick, M. Sagy, A. Wong, E. Ghassemi, D.J. Chung, D.L. Borjesson, and C.E. Yellowley. 2013. Mobilization of endogenous stem cell populations enhances fracture healing in a murine femoral fracture model. *Cytotherapy*. 15.

37. Wilson, S.S., A. Wong, C.A. Toupadakis, and C.E. Yellowley. 2015. Expression of angiopoietin-like protein 4 at the fracture site: Regulation by hypoxia and osteoblastic differentiation. *Journal of Orthopaedic Research*. 33.

38. Nguyen, P.D., and P.D. Currie. 2018. In vivo imaging: Shining a light on stem cells in the

living animal. *Development*. 145.

39. Pacini, S., and M. Petrini. 2017. In search of in vivo MSC. *Frontiers in Cell and Developmental Biology*. 5.

40. Antebi, B., L.A. Rodriguez, K.P. Walker, A.M. Asher, R.M. Kamucheka, L. Alvarado, A. Mohammadipoor, and L.C. Cancio. 2018. Short-term physiological hypoxia potentiates the therapeutic function of mesenchymal stem cells. *Stem Cell Research and Therapy*. 9:265.

41. Anderson, D.E., B.D. Markway, D. Bond, H.E. McCarthy, and B. Johnstone. 2016. Responses to altered oxygen tension are distinct between human stem cells of high and low chondrogenic capacity. *Stem Cell Research and Therapy*. 7.

42. Elabd, C., T.E. Ichim, K. Miller, A. Anneling, V. Grinstein, V. Vargas, and F.J. Silva. 2018. Comparing atmospheric and hypoxic cultured mesenchymal stem cell transcriptome: Implication for stem cell therapies targeting intervertebral discs. *Journal of Translational Medicine*. 16.

43. Kwon, S.Y., S.Y. Chun, Y.S. Ha, D.H. Kim, J. Kim, P.H. Song, H.T. Kim, E.S. Yoo, B.S. Kim, and T.G. Kwon. 2017. Hypoxia enhances cell properties of human mesenchymal stem cells. *Tissue Engineering and Regenerative Medicine*. 14.

44. Luo, Z., F. Wu, E. Xue, L. Huang, P. Yan, X. Pan, and Y. Zhou. 2019. Hypoxia preconditioning promotes bone marrow mesenchymal stem cells survival by inducing HIF-1α in injured neuronal cells derived exosomes culture system. *Cell Death and Disease*. 10.

45. Ma, T., W.L. Grayson, M. Frohlich, and G. Vunjak-Novakovic. 2009. Hypoxia and stem cell-based engineering in mesenchymal tissues. *American Institute of Chemical*

Engineering. 25.

46. Müller, J., K. Benz, M. Ahlers, C. Gaissmaier, and J. Mollenhauer. 2011. Hypoxic conditions during expansion culture prime human mesenchymal stromal precursor cells for chondrogenic differentiation in three-dimensional cultures. *Cell Transplantation*. 20.

47. Shaik, S., D. Hayes, J. Gimble, and R. Devireddy. 2017. Inducing heat shock proteins enhances the stemness of frozen-thawed adipose tissue-derived stem cells. *Stem Cells and Development*. 26.

48. Pattappa, G., B. Johnstone, J. Zellner, D. Docheva, and P. Angele. 2019. The importance of physioxia in mesenchymal stem cell chondrogenesis and the mechanisms controlling its response. *International Journal of Molecular Sciences*. 20.

49. Costantini, D. 2019. Understanding diversity in oxidative status and oxidative stress: The opportunities and challenges ahead. *The Journal of Experimental Biology*. 222.

50. Salmon, A.B., A. Richardson, and V.I. Pérez. 2010. Update on the oxidative stress theory of aging: Does oxidative stress play a role in aging or healthy aging? *Free Radical Biology and Medicine*. 48.

51. Denu, R.A., and P. Hematti. 2016. Effects of oxidative stress on mesenchymal stem cell biology. *Oxidative Medicine and Cellular Longevity*. 10.

52. Vono, R., E. Jover Garcia, G. Spinetti, and P. Madeddu. 2018. Oxidative stress in mesenchymal stem cell senescence: Regulation by coding and noncoding RNAs. *Antioxidants and Redox Signaling*. 29.

53. Zou, X., H. Li, L. Chen, A. Baatrup, C. Bünger, and M. Lind. 2004. Stimulation of porcine bone marrow stromal cells by hyaluronan, dexamethasone and rhBMP-2. *Biomaterials*. 25.

54. Zhou, X., Y. Hong, H. Zhang, and X. Li. 2020. Mesenchymal stem cell senescence and rejuvenation : Current status and challenges. *Frontiers in Cell and Developmental Biology*. 8:1–13.

55. Vitale, I., G. Manic, R. De Maria, G. Kroemer, and L. Galluzzi. 2017. DNA damage in stem cells. *Molecular Cell*. 66:306–319.

56. Chen, F., Y. Liu, N. Wong, and J. Xiao. 2017. Oxidative stress in stem cell aging. *Cell Transplantation*. 26:1483–1495.

57. Nava, M.M., Y.A. Miroshnikova, L.C. Biggs, C.M. Niessen, K.N. Dahl, S.A. Wickstro, B. Hoffmann, R. Merkel, C.M. Niessen, K.N. Dahl, and S.A. Wickstrom. 2020. Heterochromatin driven nuclear softening protects the genome against mechanical stress-induced damage. *Cell*. 181:800–817.

58. Santos, Á., A.W. Cook, R.E. Gough, M. Schilling, A. Olszok, I. Brown, L. Wang, J. Aaron, M.L. Martin-fernandez, F. Rehfeldt, and C.P. Toseland. 2020. DNA damage reorganisation alters nuclear mechanics through chromatin. *bioRxiv*.

59. Miroshnikova, Y.A., I. Cohen, E. Ezhkova, and S.A. Wickstrom. 2019. Epigenetic gene regulation, chromatin structure, and force-induced chromatin remodelling in epidermal development and homeostasis. *Current Opinion in Genetics & Development*. 55:46–51.

60. Miroshnikova, Y.A., M.M. Nava, and S.A. Wickstrom. 2017. Emerging roles of mechanical forces in chromatin regulation. *Journal of Cell Science*. 130:2243–2250.

61. Venit, T., S.R. Mahmood, and M. Endara-coll. 2020. Nuclear actin and myosin in chromatin regulation and maintenance of genome integrity. *International Review of Cell and Molecular Biology*. 6:1–42.

62. Caplan, A.I. 2015. Adult Mesenchymal Stem Cells : When , Where , and How. 2015.

63. Stavley, R., and K. Nurgali. 2020. The emerging antioxidant paradigm of mesenchymal stem cell therapy. *Stem Cells Translational Medicine*. 9:985–1006.

64. Limoli, C.L., and E. Giedzinski. 2003. Induction of Chromosomal Instability by Chronic Oxidative Stress. *Neoplasia*. 5:339–346.

65. Gonzalez-Hunt, C.P., M. Wadhwa, and L.H. Sanders. 2018. DNA damage by oxidative stress: Measurement strategies for two genomes. *Current Opinion in Toxicology*. 7:287–294.

66. Irianto, J., D.A. Lee, and M.M. Knight. 2014. Quantification of chromatin condensation level by image processing. *Med Eng Phys*. 36:412–417.

67. Ghosh, S., V.C. Cuevas, B. Seelbinder, and C.P. Neu. 2021. Image based elastography of heterochromatin and euchromatin domains in the deforming cell nucleus. *Small*. 17:e2006109.

68. Deng, P., Y. Yu, C. Hong, and C.Y. Wang. 2020. Growth differentiation factor 6, a repressive target of EZH2, promotes the commitment of human embryonic stem cells to mesenchymal stem cells. *Bone Research*. 8.

69. Verzijlbergen, K.F., A.W. Faber, I.J. Stulemeijer, and F. Leeuwen, Van. 2009. Multiple histone modifications in euchromatin promote heterochromatin formation by redundant mechanisms in Saccharomyces cerevisiae. *BMC Molecular Biology*. 10.

70. Block, T.J., M. Marinkovic, O.N. Tran, A.O. Gonzalez, A. Marshall, D.D. Dean, and X.D. Chen. 2017. Restoring the quantity and quality of elderly human mesenchymal stem cells for autologous cell-based therapies. *Stem Cell Research & Therapy*. 8.

71. Yang, Y.H.K. 2018. Aging of mesenchymal stem cells: Implication in regenerative medicine. *Regenerative Therapy*. 9.

72. Liguori, I., and G. Russo. 2018. Oxidative stress, aging, and diseases. *Clinical Intervetions in Aging*. 13:757–772.

73. Niedermaier, B., A. Sak, E. Zernickel, S. Xu, M. Groneberg, and M. Stuschke. 2019. Targeting ARID1A-mutant colorectal cancer: depletion of ARID1B increases radiosensitivity and modulates DNA damage response. *Scientific Reports*. 9.